Chem Soc Rev

REVIEW ARTICLE

View Article Online
View Journal | View Issue

Check for updates

Cite this: *Chem. Soc. Rev.*, 2020, **49**, 1144

Supramolecular materials based on AIE luminogens (AIEgens): construction and applications

Jie Li,[ab] Jianxing Wang,[ab] Haoxuan Li,[ab] Nan Song,[ab] Dong Wang*[ab] and Ben Zhong Tang *[c]

The emergence of aggregation-induced emission luminogens (AIEgens) has significantly stimulated the development of luminescent supramolecular materials because their strong emissions in the aggregated state have resolved the notorious obstacle of the aggregation-caused quenching (ACQ) effect, thereby enabling AIEgen-based supramolecular materials to have a promising prospect in the fields of luminescent materials, sensors, bioimaging, drug delivery, and theranostics. Moreover, in contrast to conventional fluorescent molecules, the configuration of AIEgens is highly twisted in space. Investigating AIEgens and the corresponding supramolecular materials provides fundamental insights into the self-assembly of nonplanar molecules, drastically expands the building blocks of supramolecular materials, and pushes forward the frontiers of supramolecular chemistry. In this review, we will summarize the basic concepts, seminal studies, recent trends, and perspectives in the construction and applications of AIEgen-based supramolecular materials with the hope to inspire more interest and additional ideas from researchers and further advance the development of supramolecular chemistry.

Received 1st December 2019

DOI: 10.1039/c9cs00495e

rsc.li/chem-soc-rev

Published on 23 January 2020. Downloaded by Yunnan University on 8/9/2025 11:18:24 PM.

1. Introduction

Life systems, such as proteins, DNA, and lipids, even complicated organisms, predominantly comprise thousands of simple molecules through intermolecular noncovalent interactions.[1,2] A widely known example is the bilayer-structured biological membrane, where amphiphilic phospholipids arrange their lipophilic chains inside the membrane and polar groups toward the aqueous medium *via* hydrophobic interactions. In order to understand and simulate such natural systems,

[a] *Center for AIE Research, College of Materials Science and Engineering, Shenzhen University, Shenzhen 518060, China. E-mail: wangd@szu.edu.cn*
[b] *College of Physics and Optoelectronic Engineering, Shenzhen University, Shenzhen 518060, China*
[c] *Hong Kong Branch of Chinese National Engineering Research Center for Tissue Restoration and Reconstruction, Department of Chemistry, The Hong Kong University of Science and Technology, Clear Water Bay, Kowloon, Hong Kong, China. E-mail: tangbenz@ust.hk*

Jie Li

Jie Li received his PhD from Peking University in 2017. Later, he joined the Center for AIE Research, College of Materials Science and Engineering, Shenzhen University, as a postdoctoral fellow. His research mainly focuses on supramolecular self-assembly, including the design and synthesis of AIEgen-based amphiphiles, as well as their self-assembly in water and biosystem applications.

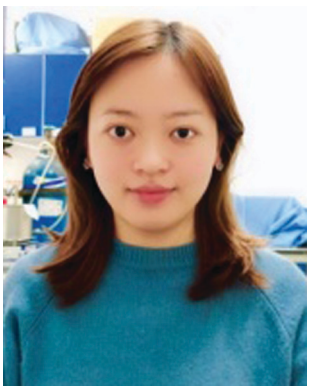

Jianxing Wang

Jianxing Wang received her PhD from the University of Science and Technology Beijing in 2019. Later, she joined the Center for AIE Research, College of Materials Science and Engineering, Shenzhen University, as a postdoctoral fellow. Her research mainly focuses on supramolecular self-assembly based on gold-based materials with AIE effects.

This journal is © The Royal Society of Chemistry 2020

Published on 23 January 2020. Downloaded by Yunnan University on 8/9/2025 11:18:24 PM.

supramolecular chemistry has emerged as a topical research field to organize minimalistic molecular building blocks to form well-defined and highly ordered architectures at various scales.[3–9] The development of this research field dates back to 1987 when the Nobel Prize was awarded to Pedersen, Cram, and Lehn for their pioneering contributions to supramolecular chemistry. Since then, this field has drawn worldwide attention, and numerous efforts have been devoted toward it. Nowadays, using nature as the inspiration, supramolecular architectures with diverse shapes, compositions, and functionalities have been successfully developed *via* various noncovalent interactions, such as hydrogen bonding, electrostatic interactions, hydrophobic interactions, and π–π interactions.[10–17] Supramolecular self-assembly has provided an innovative "bottom-up" approach *via* the elaborate design of sub-nanoscale small molecules to form well-defined nano- or microscale supramolecular architectures and consequently become one of the promising methods for use in nanoscience and nanotechnology.[18–27]

Among the various kinds of noncovalent interactions, supramolecular architectures constructed on the basis of π–π interactions show distinctive properties by introducing conjugated luminescent molecules into the supramolecular systems. These lightened supramolecular architectures have received tremendous attention due to their promising potential in many fields such as optical nanodevices, drug/gene delivery, sensors, and cellular imaging.[28,29] In principle, luminescent molecules usually contain large amounts of conjugated aromatic rings with highly planar configurations. These planar molecules possess the adaptive capacity of strong π–π stacking interactions, resulting in an intrinsic tendency to form stable and ordered structures.[30,31] Evidently, most of the reported supramolecular materials are fabricated by conjugated planar molecules, such as perylene and its derivates. However, the strong intramolecular π–π interaction also typically leads to the formation of enormous excimers or exciplexes in aggregated or solid states, which severely quench fluorescence emissions. As a result, fluorescence emissions are usually extremely weak or completely negligible in supramolecular structures. This aggregation-caused quenching (ACQ) effect is common in most conjugated fluorescent molecular systems, and it adversely impacts the practical applications of supramolecular luminescent materials.[32] Therefore, there is an intrinsic obstacle for current conjugated fluorescent molecules to construct supramolecular materials with high luminescence efficiency.

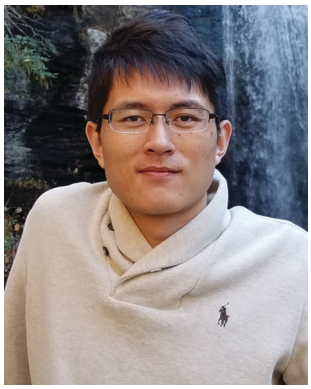

Haoxuan Li

Haoxuan Li received his PhD in Nonwoven Materials and Engineering at Donghua University, China, in 2018. He joined the Xia group at Georgia Institute as a visiting graduate student under the supervision of Prof. Younan Xia in 2015. Now, he is conducting his postdoctoral work on the development of functional luminescent materials with aggregation-induced emission characteristics and exploration of their applications in wearable flexible materials and solar-induced water evaporation applications in Prof. Ben Zhong Tang's group.

Nan Song

Nan Song received her degrees (BSc, 2013; PhD, 2018) from Jilin University, where she performed research under the direction of Professor Ying-Wei Yang and majored in organic chemistry. She was also as a joint PhD candidate at UCLA from 2016 to 2017 under the supervision of Prof. Paul S. Weiss. In 2019, she undertook postdoctoral training at Shenzhen University and Hong Kong University of Science and Technology in collaboration with Prof. Ben Zhong Tang and Prof. Dong Wang. Her research interests are focused on pillararene-based supramolecular chemistry, multifunctional hybrid nanomaterials, and optical supramolecular materials.

Dong Wang

Dong Wang received his PhD from Bordeaux University, and he conducted his postdoctoral study at the University of Toronto and HKUST. He is currently an associate professor in Shenzhen University. His research focuses on the design of AIEgens for chemical sensing and biological applications.

Ben Zhong Tang

Ben Zhong Tang received his PhD from Kyoto University. He conducted his postdoctoral research at the University of Toronto. He joined HKUST in 1994 and was promoted to Chair Professor in 2008. He was elected to the Chinese Academy of Sciences in 2009. He is now serving as the Editor-in-Chief of Materials Chemistry Frontiers.

Published on 23 January 2020. Downloaded by Yunnan University on 8/9/2025 11:18:24 PM.

Fortunately, an unusual phenomenon, precisely opposite to the ACQ effect and termed as aggregation-induced emission (AIE), was discovered by our group in 2001.[33] The molecules with the AIE effect are nonemissive in the dispersed state, but they are intensively luminescent in the aggregate form (including amorphous aggregates and ordered aggregates) or solid state, enabling high fluorescence in supramolecular structures. Since AIE luminogens (AIEgens) usually consist of flexibly rotated or vibrated molecular moieties, they can consume the energy of the excited state upon photoexcitation through intramolecular motion in the dispersed state. However, in the aggregated state, such motion is spatially restricted; therefore, AIEgens follow the radiative pathway to dissipate the absorbed energy, exhibiting distinct fluorescence emissions.[34–36] The restricted intramolecular rotation (RIM) mechanism is applicable to almost all the reported AIE systems. Taking HPS as the example, the six phenyl peripheries are linked to a silole core *via* single bonds.[37] In a dilute solution, the strong molecular rotations cause the energy consumption of the excited state *via* nonradiative pathways. In the aggregated state, such rotations, however, are restricted due to physical constraints that block the nonradiative pathway and therefore enable the excitons to radiatively decay. Moreover, several other mechanisms such as J-aggregates formation,[38] conformational planarization, suppression of twisted intermolecular charge transfer (TICT), *E*/*Z* isomerization, and realization of excited-state intramolecular proton transfer (ESIPT), can also be responsible for AIE.[36] Further, in certain cases, enhanced emissions in aggregates are caused by the synergetic effect of multiple mechanisms. Remarkable progresses have been made in the past decades that have exceedingly stimulated the development and utilization of AIEgens as self-aggregates in most cases, as well as AIEgens-containing systems (such as AIEgens-containing host–guest complexes) in which the intramolecular motion of AIEgens is considerably restricted by the limited space.[36] The intrinsic features of AIEgens perfectly permit their use as aggregates in luminescent supramolecular materials. Moreover, the AIE features endow a fluorescence turn-on nature when AIEgens spontaneously aggregate in a hydrophilic environment or conjugate with analytes, yielding higher sensitivity and excellent signal-to-noise ratio.[39–41] Furthermore, AIEgens also possess additional impressive functions, such as the generation of reactive oxygen species (ROS), photothermal conversion, and fluorescence sensing upon assembly or disassembly.[42–48] Combining with other distinct advantages such as large Stokes shift and structural diversity, the utilization of AIEgens has sparked intense research interest and opened up a venue to achieve a series of possibilities for luminescent supramolecular materials.

The development of AIEgen-based supramolecular materials undoubtedly pushes supramolecular chemistry forward, because the AIE effect not only realizes the construction of supramolecular materials with high luminescence efficiency, but also involves newer applications of supramolecular materials in a large range of fields such as optical devices and biosystems. AIEgen-based supramolecular materials are generally fabricated *via* a simple assembly approach, wherein building blocks are combined that spontaneously form highly ordered architectures through noncovalent interactions. The large variety and reversibility of noncovalent interactions drastically decrease the workload and difficulty of preparation, thereby enabling luminescent supramolecular materials with diverse morphologies and controlled and tunable architectures, as well as materials that can respond to external stimuli. In addition, traditional techniques to observe the structural or morphological changes in materials science are based on electron microscopy, such as atomic force microscopy (AFM) and transmission electron microscopy (TEM).[49–52] These methods, however, often suffer from several drawbacks. For instance, dehydration in the preparation and scanning process always destroy the supramolecular structure, resulting in inaccurate results. Moreover, the operating environment of the electron microscope makes it impossible to obtain real-time and onsite visualization. Confocal laser fluorescence microscopy (CLSM) has been proven to be a simple and feasible method with high sensitivity and capable of onsite and real-time evaluation. The integration of fluorescence in supramolecular materials opens up an additional avenue for CLSM in the visualization of supramolecular structures and their transitions.[53] The high luminescence efficiency of AIEgen-based supramolecular materials allows us to gain straightforward insights into the fundamental information of supramolecular structures and monitor their real-time formation and transition processes.

Because of these unique advantages, increased attention has been focused on AIEgen-based supramolecular materials in the recent decades. Because of this worldwide attention, a large variety of luminescent supramolecular materials based on AIEgens have been developed, and a number of practical applications have been explored. In this review, we try to offer an integrated perspective through the introduction and discussion of new breakthroughs and trends in the area of supramolecular materials based on AIEgens. We will discuss the mechanistic insights into AIE molecular configurations and the construction of diverse supramolecular structures, involving macrocycle, ordered self-assembly, and macromolecular systems. In addition, their applications in specific sensor, delivery, and fundamental research with regard to materials science will be demonstrated. Finally, with the aim of stimulating new development in this exciting area of research, we will give a perspective on future works.

2. Construction of AIEgens-based supramolecular materials

Since the discovery of the AIE phenomenon in 2001, efforts have been globally devoted toward the development of AIE research. Until now, a substantial number of AIE molecules with different skeletons, emission colors, and functionalities have been designed and reported. In contrast to traditional disc-like planar fluorescent molecules, these AIE molecules share a common structural feature, namely, nonplanar configuration.[54] Typical examples are tetraphenylethene (TPE)

 This journal is © The Royal Society of Chemistry 2020

Published on 23 January 2020. Downloaded by Yunnan University on 8/9/2025 11:18:24 PM.

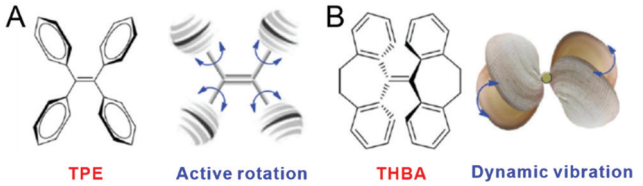

Fig. 1 Typical examples of nonplanar configurations of AIEgens. (A) Propeller-shaped TPE and its intramolecular rotation. (B) Shell-like THBA and its intramolecular vibration. Reproduced with permission from ref. 35. Copyright 2014 Wiley-VCH.

and 10,10′,11,11′-tetrahydro-5,5′-bidibenzo[*a*,*d*][7]annulenylidene (THBA). TPE molecules usually adopt a propeller-shaped structure, where four phenyl rings are connected to the central ethene rod *via* single bonds with large torsion angles (Fig. 1A). In the dispersed state, the four phenyl rings of TPE can freely rotate, opening a relaxation channel of molecular rotation to dissipate the energy of the excited states. Similarly, the THBA molecule is composed of two noncoplanar portions, where the two phenyl rings are linked and locked by a bendable flexure (Fig. 1B).[55] This anti-conformation allows the phenyl rings of THBA to dynamically bend or vibrate in the solution, similar to the breathing movement of a clam or scallop. The intramolecular vibration of THBA is another relaxation pathway for its excited states toward nonradiative decay. Upon aggregation, physical constraints and space limitations can considerably restrict the intramolecular rotation or vibration of AIEgens. As a result, the radiationless pathway is locked and the radiative decay channel is opened, which renders AIEgens to become efficiently emissive in the aggregated state.

The unique nonplanar configuration endows AIEgens with promising potential toward the fabrication of luminescent supramolecular materials. However, this highly twisted or propeller-shaped molecular conformation either prevents the face-to-face packing of AIEgens or hampers the intermolecular π–π stacking interaction in space. Therefore, the key to fabricate AIEgen-based luminescent supramolecular materials is to ensure AIEgens with sufficient aggregation ability to form the supramolecular architectures. A popular strategy typically involves the decoration of AIEgens with various moieties that possess a strong tendency of aggregation, such as hydrophobic alkyl chains, biomolecules, amphiphiles, and polymers, *via* covalent or noncovalent pathways. For instance, four long alkyls can be linked to the TPE core, which can significantly increase the hydrophobic interaction and result in the formation of a fibrous structure.[56] An alternate protocol is the incorporation of AIEgens into pre-prepared supramolecular structures. The strong stability and self-assembly capacity of supramolecular materials trigger AIEgens to organize into well-defined and ordered supramolecular morphologies. Based on the above two strategies, a large number of AIEgen-based supramolecular luminescent materials with diverse architectures at all scales have been developed in the recent years. In this section, we summarize the progress on the construction of AIEgen-based supramolecular materials with some typical examples, including macrocycle, self-assembly, and macromolecular systems.

2.1. Macrocycle systems

Macrocycles, such as crown ethers, cyclodextrins (CDs), calixarenes, cucurbiturils (CBs), and pillararenes, are types of molecules with intrinsic cavities in which guests can be embedded *via* noncovalent interactions. As guest molecules perfectly match the cavity size of the host macrocycle, host–guest systems possess unique molecular recognition performance and play a vital role in the construction of supramolecular luminescent materials.[57–62]

In principle, the fluorescence of AIEgens is generated due to the restriction of intermolecular motion. Therefore, the straightforward strategy for macrocycle systems to build supramolecular luminescent materials involves the encapsulation of AIEgens into the cavities of macrocycles, where the limited space restricts the rotation or variation of AIEgens and amplifies fluorescence emissions. A typical example is single-molecule luminogens obtained by covalently binding TPE to CDs.[63] In CDs, hydrophilic glucopyranose units are connected with a nonsymmetrical bucket-like cyclic configuration. The CD molecules are soluble in an aqueous solution, while their inner cavities are hydrophobic. As a result, insoluble organic TPE segments can enter the cavity to form supramolecular complexes through the hydrophobic effect (Fig. 2A). Fig. 2 shows the phenyl rings of TPE located in the CD cavity, where the limited space restricts motion and hence the fluorescence of TPE is turned on. Since a smaller cavity (α-CD) can restrict the motion of phenyl rings more efficiently than the larger ones (β-CD or γ-CD), the TPE trapped in α-CD showed a stronger fluorescence emission at 410 nm and higher quantum yield than those obtained from β-CD and γ-CD under the same conditions (Fig. 2B and C). Because of these advantages of high emission efficiency and good biocompatibility, TPE–CD complexes exhibited outstanding performance for biological imaging in living cells.

In addition to covalent pathways, AIEgens can also combine to macrocycle molecules *via* noncovalent interactions. Cao and coworkers[64] reported a supramolecular luminescent rotaxane by the inclusion complexes of cucurbit derivate CB[10] and a dumbbell-like AIEgen. CB[10] is a pumpkin-shaped macrocyclic molecule with a rigid hydrophobic cavity and two identical carbonyl fringed portals. The AIEgen contains a viologen unit in the middle for binding CB[10], and two TPE units at both the terminals functioning as the stopper and fluorophore. The extremely large cavity size enabled CB[10] to thread through large-sized TPE units, particularly combining with the viologen unit *via* host–guest interactions (Fig. 2D). Meanwhile, as revealed from the nuclear magnetic resonance (NMR) measurements, one phenyl ring of each TPE unit was also anchored inside the cavity of CB[10]. The resultant restriction of the intramolecular rotation of TPE induced an obvious turn-on yellow emission (λ_{em} = 558 nm). Interestingly, in other CB[*n*] (*n* = 6–8) systems, no fluorescence emission could be observed (Fig. 2E) because the cavities of these CBs were actually smaller than the size of the TPE unit such that they failed to cross the TPE terminals to form host–guest supramolecular complexes.

In a host–guest system, AIEgens can serve as hosts to form supramolecular luminescent materials, too. This special

Published on 23 January 2020. Downloaded by Yunnan University on 8/9/2025 11:18:24 PM.

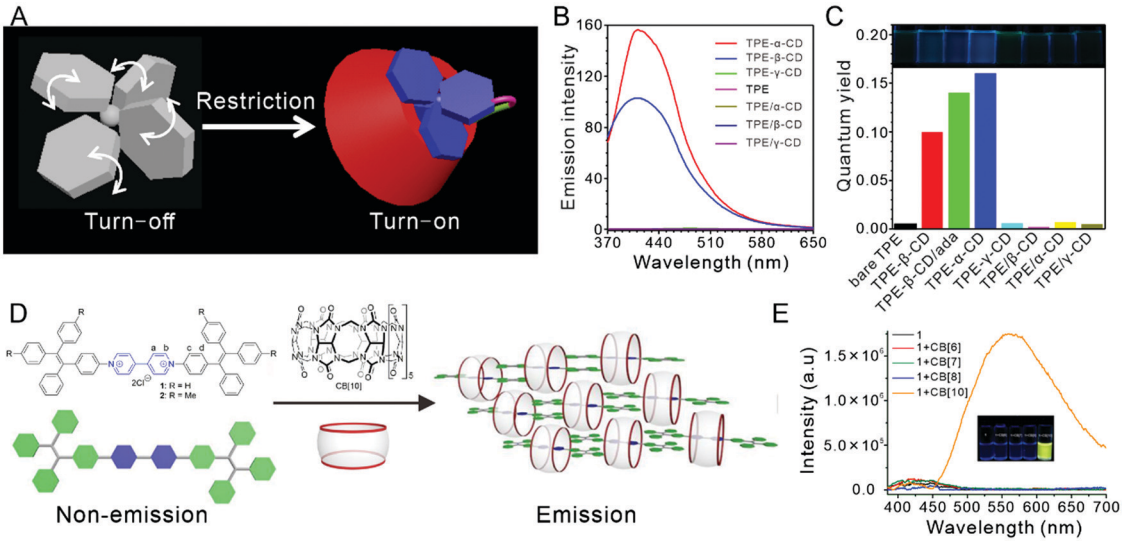

Fig. 2 AIEgens as guests in supramolecular complexes. (A) Schematic illustration of TPE guests trapped inside the cavity of CDs. (B) Fluorescence spectra and (C) quantum yield of TPE–CDs, bare TPE, and TPE–CD mixtures. Reproduced with permission from ref. 63. Copyright 2014 Royal Society of Chemistry. (D) The formation of CB[10] and dumbbell-like AIEgen complexes. (E) Fluorescence spectra of AIEgens without and with various CB[*n*] (*n* = 6–8, 10). Reproduced with permission from ref. 64. Copyright 2017 American Chemical Society.

strategy to fabricate AIEgen-based supramolecular materials can stimulate the development of various AIE-based macrocycles. For instance, Zheng and coworkers[65] synthesized a TPE Schiff base macrocycle (Fig. 3A). This macrocycle aggregated into a fibrous structure in poor solutions and hence exhibited a strong fluorescence emission due to the restriction of molecular rotation in the aggregated state (Fig. 3B). Owing to the perfect size matching to the cavities and strong binding interactions with Schiff bases, copper ions were selectively combined to this TPE-containing macrocycle. The obtained host–guest complexes induced the TPE macrocycles solution to undergo an obvious color change from colorless to yellow associated with an intense quenching of fluorescence emission (Fig. 3C). This specific combination between the TPE macrocycle and copper ions could be used to build ultrasensitive and selective sensors for the detection of copper ions.

Recently, our group[66] reported an elegant AIE-active host with a 3D cage structure (Fig. 3D). This cage was prepared by covalently binding two propeller-shaped AIE molecules of tetraphenylpyrazine (TPP) to the *para* position of triglycol monomethyl ether-substituted triazine. Unlike other AIE-based macrocycles, this 3D TPP-Cage emitted strong and deep blue fluorescence in dilute solutions since all the four phenyl rings of TPP were immobilized in the cage and therefore the intramolecular rotations of the TPP unit were efficiently restricted. Because of the large and hydrophobic cavity of the TPP-Cage, many organic guest molecules with proper sizes, even for traditional ACQ fluoregens, could be encapsulated to construct host–guest-based supramolecular materials with excellent luminescence properties. For instance, DPP is a well-known yellow-emissive conjugated compound and shows the ACQ effect. Its yellow emission can be quenched in an aqueous medium due to the formation of aggregates. When DPP is threaded into the cavity of TPP-Cage in an aqueous solution or in the aggregated state to form a host–guest complex, strong emission still persists. This is because the TPP-Cage serves as an inherent block to separate DPP molecules, where the strong π–π stacking could be prevented and no aggregates were formed. In addition to the blue emission from TPP-Cage and yellow emission from DPP, the complex exhibited a stable white-light emission. Such an excellent example provides a new approach to overcome the obstacle of the ACQ effect, as well as a platform to fabricate supramolecular luminescent materials.

In addition to the utilization of AIEgens as hosts or guests, host–guest complexes can also act as building blocks to connect AIEgen-containing groups, yielding supramolecular materials. This strategy has been substantially applied in a large range of research in nanotechnology and materials science, such as dynamic supramolecular polymers, nanoparticles, films, and gels. For example, our group[67] fabricated a host–guest supramolecular polymer by using AIEgens and CBs. CBs have high binding capacity with a variety of positively charged guests. As shown in Fig. 4, AIEgens can, therefore, be designed to possess two positively charged segments (A and B), which enables them to connect with two CBs. On account of the relatively large cavity of CB[8], two positively charged segments from individual AIEgens can be properly encapsulated inside the cavity. As a result, the AIEgens and CB complexes can be further assembled into linear supramolecular polymers. The formation of this supramolecular polymer undergoes a two-step process. The first step is the formation of homoditopic AA and BB ternary complexes, which act as supramonomers. The second step involves the formation of supramolecular polymers by supramonomers through self-sorting. Interestingly, the formed AB complexes can be spontaneously corrected into AA or BB units during supramolecular polymerization. This is because

 This journal is © The Royal Society of Chemistry 2020

Published on 23 January 2020. Downloaded by Yunnan University on 8/9/2025 11:18:24 PM.

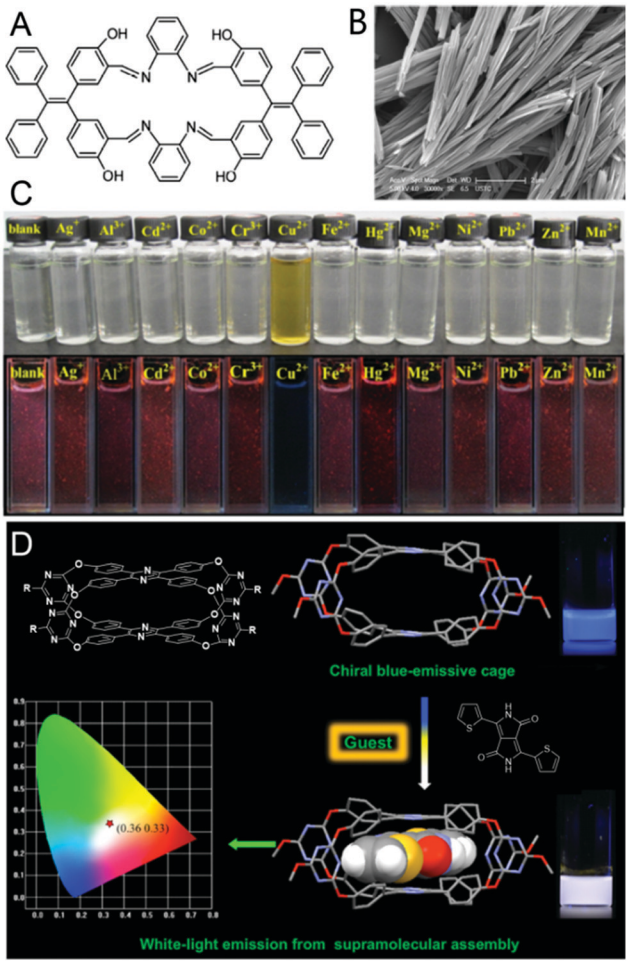

Fig. 3 AIEgens as hosts in supramolecular complexes. (A) Chemical structure of TPE-containing macrocycle and its aggregated morphology (B). (C) Photographs of TPE-containing macrocycle solution under daylight and 365 nm light after the addition of metal ions. Reproduced with permission from ref. 65. Copyright 2014 Royal Society of Chemistry. (D) The formation of supramolecular assembly of host (TPP-Cage) and guest. Reproduced with permission from ref. 66. Copyright 2018 American Chemical Society.

the outcome can be thermodynamically controlled, where the AB units are relatively unstable on the chains and can break up and gradually transform into more stable AA or BB units due to chain rigidity and unfavorable entropy reduction. Since the two segments of AIEgens can be encapsulated by CB[8] in the polymer chain, the molecular motion is considerably restricted, leading to a large reduction in nonradiative decay. Therefore, supramolecular polymers exhibit obvious fluorescence.

Liu and coworkers[68] presented an example of AIEgens-based fluorescent nanoparticles with the macrocycle sulfonatocalixarene (SCnAs). SCnAs is a well-known host molecule with π-electron-rich cavities and has been widely used in molecular recognition, sensing, and self-assembly applications. This AIEgen was fabricated by modifying the TPE moiety with two quaternary ammoniums (Fig. 5A). The resultant highly positive charges from quaternary ammoniums enabled AIEgens to effectively dissolve in water, as well as the intriguing inclusion into SCnAs or bisSC4A. The formation of TPE–SCnAs or bisSC4A complexes lowered the critical aggregation concentration (CAC) of AIEgens, enhanced their aggregate stability, and regulated the degree of order in their aggregates (Fig. 5B). In this work, the host–guest interaction between quaternary ammoniums and SCnAs promoted the aggregation capacity of AIEgens, rendering the AIEgens to form ordered supramolecular structures.

AIEgens can also self-assemble into a variety of 3D macroscopic supramolecular structures based on host–guest interactions. For example, Cao and coworkers[69] constructed 3D fluorescent supramolecular organic frameworks by using CB[8] and AIEgens in water (Fig. 6). The AIEgen consisted of a central TPE core and four pyridinium(vinyl) arms at the terminals. Since each CB[8] molecule encapsulated two pyridinium(vinyl) arms in its cavity from neighboring AIE molecules, the host–guest complexes stacked in a head-to-tail pattern, leading to the formation of 2D supramolecular network layers. Interestingly, when the TPE core was covalently linked to pyridinium(vinyl) by rigid linkers, the 2D network layers were planar and parallelly stacked together, producing a supramolecular cuboid structure. However, spheroids were obtained when AIEgens contained flexible and rotatable linkers. This was because the linkers of complexes were usually bent to reduce their energy and therefore formed curved supramolecular network layers, which further aggregated and generated supramolecular spheroids with minimum energy. As the TPE motifs were tightly stacked in the network and their rotations were considerably restricted, these supramolecular 3D materials exhibited outstanding fluorescence emissions in water, and they found applications in cellular imaging. Huang and coworkers[70] fabricated a fluorescent supramolecular film with pillar[5]arene-based polymers. In this polymer, the TPE segment was positioned in the main chain and the macrocycle pillar[5]arene was placed in the side chains. Based on the strong host–guest interactions between the symmetric crosslinker and pillar[5]arene, TPE-containing conjugated polymers were crosslinked and self-assembled into fluorescent films, where the intramolecular motion of TPE units was strongly restricted. Yang and his group[71] reported a supramolecular fluorescent gel obtained *via* host–guest interactions, where the TPE-bridged pillar[5]arene tetramers interacted with the triazole-based neutral linkers. The rotations of the TPE segments were spatially restricted by the crosslinked structure of the gels, rendering the gels with strong blue fluorescence.

It is noteworthy that crown ethers have attracted considerable attention for applications in supramolecular chemistry due to the host–guest recognition of crown ether toward different guest species, including potassium ions, ammonium, and paraquat derivatives.[72] Several AIEgen-based supramolecular materials have been fabricated with crown ethers. Taking dibenzo[24]crown-8 as an example, we designed and synthesized two TPE-derivatives, namely, dibenzo[24]crown-8 moieties (TPE-DDBC) and benzylamino groups (TPE-DBA), performing as the host and guest molecules, respectively (Fig. 7A).[73] In an acidic environment, the protonated secondary amine units in TPE-DBA specifically reorganized to the crown ethers of TPE-DDBC, leading to the formation of a complex that further

Published on 23 January 2020. Downloaded by Yunnan University on 8/9/2025 11:18:24 PM.

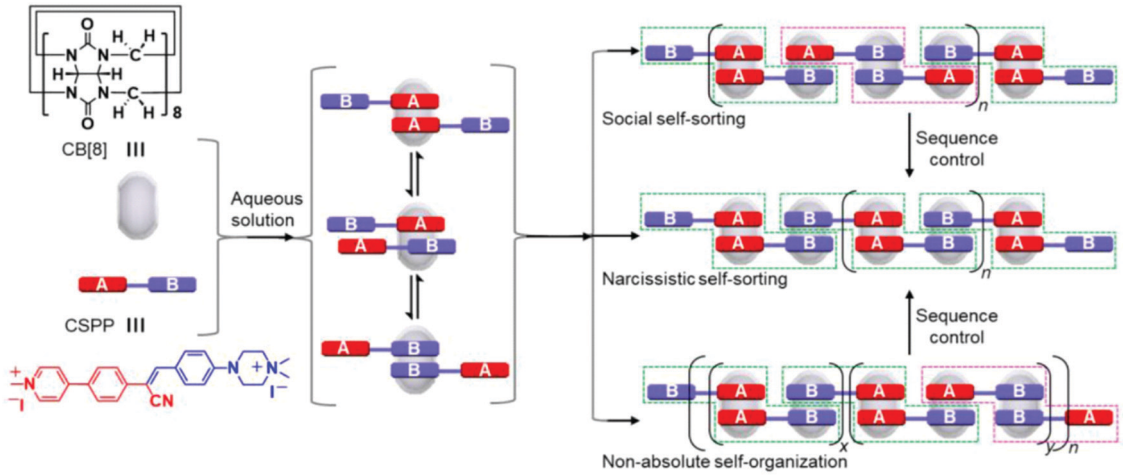

Fig. 4 Illustration of the dynamic self-sorting formation of the supramolecular 1D polymers of CB[8] and AIEgens. Reproduced with permission from ref. 67. Copyright 2019 American Chemical Society.

self-assembled into lamellar aggregates (Fig. 7B). These lamellar aggregates showed strong emissions due to the restriction of rotation of the TPE groups. Because of the dynamic and reverse ability of host–guest interactions, the complexes disassembled and their emission faded under basic conditions because the deionized amines could not be hosted by crown ethers, and the restriction effect disappeared. This fluorescence "turn-on/turn-off" behaviors were reversible, and they could be adjusted by the stepwise addition of HCl and NaOH (Fig. 7C and D). The emissions became stronger and blue-shifted after every cycle. This might be associated with the formation of NaCl salt during the stepwise addition of HCl and NaOH in the mixture, resulting in tighter packing of the hydrophobic TPE moieties. Therefore, a higher-ordered microstructure was formed, where the TPE moiety showed more twisted conformation.

Yin and his group[74] prepared a crosslinked supramolecular network with both AIE and ACQ chromophores based on crown systems, which exhibited different strong emissions in the aggregated or dispersed states. Here, 24-crown-8 (DB24C8) and ACQ terpyridine chromophores were linked to each side of an AIE-based TPE segment. The host–guest interactions of the crowns enabled the AIEgens to link with polymers, and the coordination between terpyridine and Zn^{2+} resulted in the formation of networks through a complex self-assembly process. The networks further transformed into gels at higher concentrations, yielding strong emissions at 460 nm due to the restriction of intermolecular rotation of the TPE group. Upon the introduction of external stimuli, such as Cl^{-}, pH, and cyclen, the gel disassembled due to the destruction of either metal coordination or host–guest interactions, and it efficiently emitted at 390 nm due to the presence of free terpyridine. The obvious color changes in the fluorescence prompted the application of supramolecular networks in advanced sensor materials.

2.2. Self-assembly systems

Self-assembly, a spontaneous process where small molecules organize into well-defined structures, is inspired from natural molecules such as DNA, lipids, and enzymes. It has emerged as the prevalent approach to fabricate supramolecular materials through various noncovalent interactions such as electrostatic interactions, hydrogen bonding, and hydrophobic effects.[75–81] Although the twisted nonplanar configuration of AIEgens is fairly harmful to their ordered stacking, self-assembly offers a series of possibilities to overcome this obstacle by enhancing the aggregating capacity of AIEgens. Therefore, a large number of supramolecular luminescent materials with well-defined morphologies have been designed and presented on the basis of AIEgens. Here, some typical and elegant examples are discussed.

Vesicular morphology is a well-known example of self-assembled supramolecular architectures. It is formed by the highly ordered organization of amphiphiles into 3D hollow structures that are widely applied in sensors, drug delivery, nanomaterials, and artificial biological membranes.[82–84] The key to trigger AIEgens into ordered stacking and well-defined vesicular architecture is to considerably increase the hydrophobicity of AIEgens. Following this design strategy, Yan and coworkers[85] fabricated an enzyme-responsive fluorescent vesicle in water through the self-assembly of the TPE-BPA AIEgen. This AIEgen contained eight negative charges, which enabled it to combine eight positively charged amphiphiles to form neutral complexes (Fig. 8A). The resultant extremely high hydrophobicity prompted ordered stacking in TPE-BPA, finally forming a vesicular structure. Since TPE-BPA was restricted in the vesicle membranes, these vesicles showed an excellent green emission in water. However, upon the addition of an enzyme into such a vesicles solution, the fluorescence emission became weakened over time because of the gradual breakdown of the vesicular structure (Fig. 8B and C). This was because the alkyl chain was cut off by the enzyme, resulting in a drastic decline in hydrophobicity. Such weak hydrophobicity could not enable an ordered arrangement in TPE-BPA and vesicles were not observed.

By using the same strategy, Li and coworkers[86] fabricated AIEgens-containing vesicles based on natural amphiphilic molecules. Bile acids are natural compounds with important roles in the biological processes of dissolving fats in living organisms.

 This journal is © The Royal Society of Chemistry 2020

Published on 23 January 2020. Downloaded by Yunnan University on 8/9/2025 11:18:24 PM.

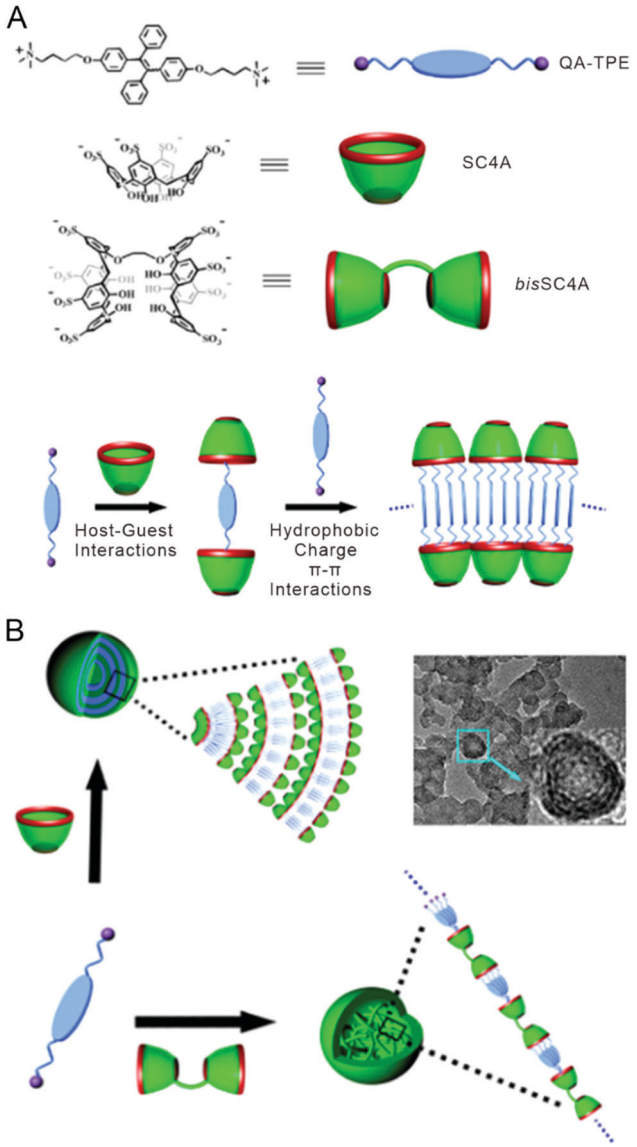

Fig. 5 Illustration of the formation of supramolecular nanoparticles. (A) Chemical structures of AIEgens and hosts, as well as their aggregation behaviors. (B) Assembly process of supramolecular nanoparticles by AIEgens and SC4A/bisSC4A. Reproduced with permission from ref. 68. Copyright 2014 American Chemical Society.

These molecules have a rigid nonplanar steroidal skeleton with a convex hydrophobic region and a concave hydrophilic face, which enable them to self-assemble in a specific arrangement, serving as powerful building blocks to create various supramolecular architectures. In such AIEgens, two bile acids were conjugated to the TPE segment. Because of the outstanding arrangements of bile acid segments *via* hydrogen bonding and hydrophobic effect, such bile-acids-conjugated TPE self-assembled into bilayer-structured vesicles. The TPE groups were tightly stacked together and exhibited strong turn-on emissions due to the restriction of intramolecular rotations in TPE.

Recently, the novel crystalline nanospherical morphology based on AIEgens was successfully formulated by supramolecular self-assembly.[87] In such AIEgens, three TPE moieties covalently combined with four cationic pyridinium units (Fig. 9A), which showed orange fluorescence with a quantum yield of 19.7% centered at 595 nm in acetonitrile. Upon the addition of the poor-solvent water, these AIEgens formed aggregates, resulting in intense enhancement in their emission intensities at 580 nm and a quantum yield as high as 97.7% could be obtained at a water fraction of 99% (Fig. 9B). The high-resolution transmission electron microscope (HRTEM) images revealed that the aggregates possessed high hexagonal order and crystalline nature (Fig. 9C). This is because the solubility of AIEgens was so poor in water that the AIEgens were intensely stacked with each other, resulting in a highly ordered arrangement. Moreover, organic dye molecules could be dispersed within the crystalline nanospheres and were located at a proper distance with the donors to achieve energy transfer (Fig. 9D), enabling crystalline nanospheres to perform as excellent well-defined supramolecular light-harvesting systems.

Supramolecular self-assembly is also a favorable approach for fabricating helical architectures because it can magnify molecular chirality to the preferred supramolecular helicity.[88–90] Chiral amino acids induce chirality and possess strong supramolecular self-assembling capabilities, making them the ideal moieties for fabricating helical structures. The incorporation of chiral amino acids units into AIEgens can induce the AIEgens to form supramolecular helical assemblies. Based on this strategy, our group[91] successfully fabricated fluorescent helical microfibers based on AIEgens and directly visualized their helicity for the first time. In such AIEgens, two leucines (Leu) were attached to the silole by the azide–alkyne "click" reaction. Silole-Leu was nonemissive in DMSO and highly emissive at 360 nm when the water fraction was more than 90%. Because of the hydrogen bond and asymmetric centers, the chiral Leu directed Silole-Leu to self-assemble into helical fibers. It was confirmed that bonding with only one amino acid could also efficiently induce AIEgens to self-assemble into helical nanofibers. The TPE-Leu AIEgen connecting one Leu to the TPE segment through a "click" reaction has been syntheszied.[92] This AIEgen formed well-defined right-handed helical nanofibers under the guidance of Leu, and it showed strong luminescence due to the restriction of intermolecular rotation of the TPE moieties. Recently, our group[93] visualized the dynamic self-assembly process of helixes based on a chiral AIEgen of Au(I) complexes (Fig. 10A). The Au(I) complexes were effectively dissolved in tetrahydrofuran (THF) and no aggregates were found. The addition of poor-solvent water enabled Au(I) complexes to aggregate together to form helical structures that showed extremely strong orange emissions at 560 nm (Fig. 10B). The SEM and AFM results (Fig. 10C) demonstrated that these aggregates underwent a morphological transformation from vesicles to helixes. Probably, the addition of a large amount of a poor solvent rendered the Au(I) complexes to form intensely stacked vesicular structures. The vesicles were thermodynamically unstable; therefore, they fused with each other and their morphologies transformed into a helical structure in order to reach a stable state over time. This morphological transitional process proceeded in a time

Published on 23 January 2020. Downloaded by Yunnan University on 8/9/2025 11:18:24 PM.

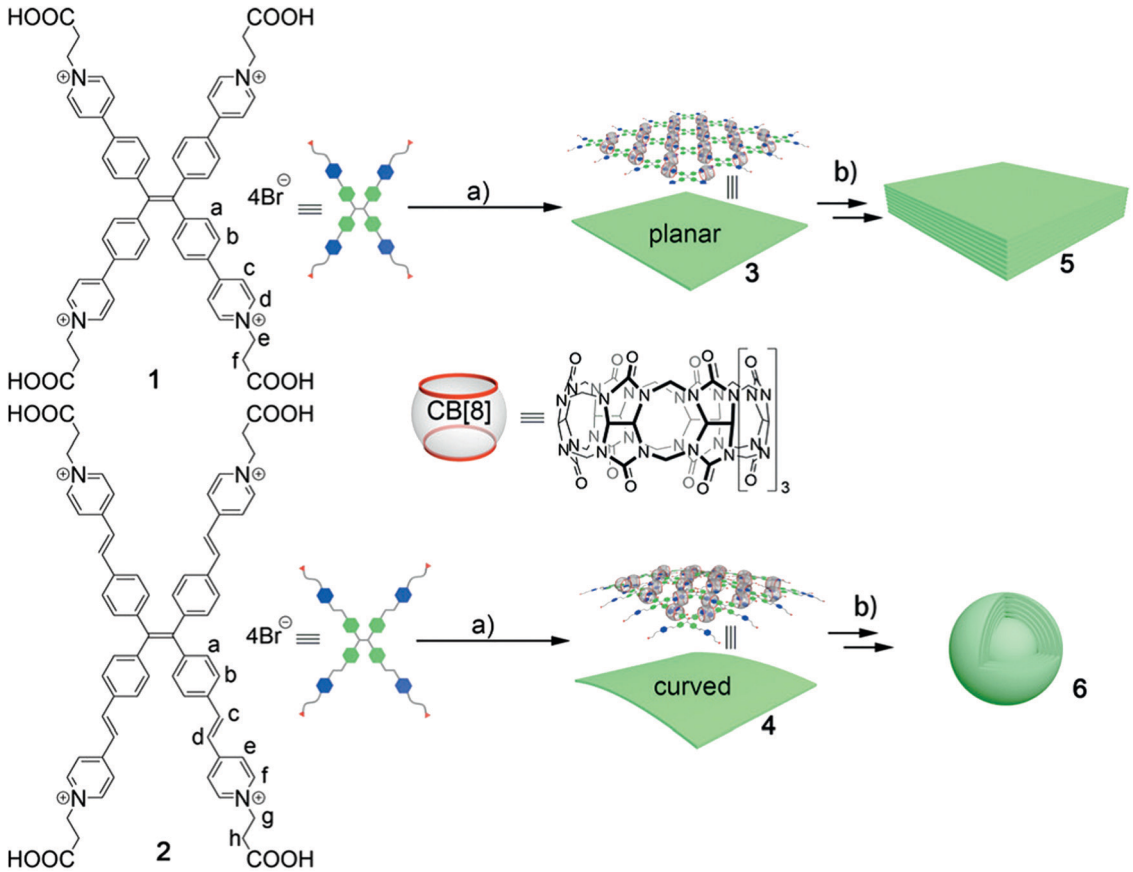

Fig. 6 Illustration of the formation of supramolecular 3D architectures. Chemical structures of two AIEgens (1 and 2) and CB[8], and the representations of the hierarchical formation of supramolecular network-type layers (3 and 4) and frameworks (5 and 6): (a) host–guest complexation; (b) stacking or aggregating. Reproduced with permission from ref. 69. Copyright 2018 Wiley-VCH.

scale of hours, offering the possibility of monitoring the morphological transition and helical formation.

Interestingly, controlling the spatial configuration of one molecule is a potentially alternate strategy to obtain supramolecular self-assemblies with diverse architectures. Since a marginal difference in the molecular formula can affect the intrinsic molecular configuration, supramolecular complexes comprising thousands of single molecules can considerably magnify the differences in supramolecular structures. Isomers are molecules with identical molecular formulas, but they have different configurations; isomers have been widely explored to fabricate supramolecular materials with different morphologies.[94–96] Our group[97] successfully fabricated two kinds of supramolecular self-assemblies with TPE-based geometric (*Z*)- and (*E*)-isomers (Fig. 11). Two TPE stereoisomers were prepared by modifying ureidopyrimidinone (UPy) into TPE moieties. The quadruple hydrogen bonding of UPy promoted the TPE stereoisomers to effectively organize into aggregates, which showed distinct fluorescence in the aggregated state. In (*Z*)-TPE–UPy, since the bulky UPy units were located on the same side of the double bond, dimer or oligomers were energetically favorable and further self-assembled into spheres in a random or loose arrangement due to their bent structures, exhibiting green emission at 495 nm. On the contrary, the UPy units were located on opposite sides in (*E*)-TPE–UPy. The molecules suffered little constraint in UPy dimerization, resulting in the formation of long and linear supramolecular polymers. This enabled them to have good packing in the aggregated state, yielding a highly ordered fiber structure and a blue emission at 479 nm. This demonstrated that a subtle change in the TPE configuration can have a considerable impact on the self-assembly behavior of the resulting molecule.

Moreover, the self-assembly strategy could be used to form macroscopic 3D supramolecular structures, such as gels and films. More recently, Liu and coworkers[98] presented a supramolecular self-assembly method to fabricate nanotube gels with AIEgens that could not aggregate into nanotubes (Fig. 12A). In this system, stable hexagonal nanotubes with obvious stability were individually built by a C_3 symmetrical L-glutamic-acid-based compound (TMGE). On account of the large amount of inner space within the assembled nanotubes, a wide range of AIEgens with different colors, such as TPE, HPS, and α-DC, could be efficiently encapsulated *via* noncovalent ways and orderly arranged along the TMGE-based nanotubes, making AIEgens coassemble into nanotubes (Fig. 12B and C). The supramolecular structure of AIEgens was directed by the morphologies of TMGE-based nanotubes gel. Since the TMGE-based nanotubes gels were chiral gels, the coassembled AIEgen gels showed excellent circularly polarized luminescent (CPL) signals.

 This journal is © The Royal Society of Chemistry 2020

Published on 23 January 2020. Downloaded by Yunnan University on 8/9/2025 11:18:24 PM.

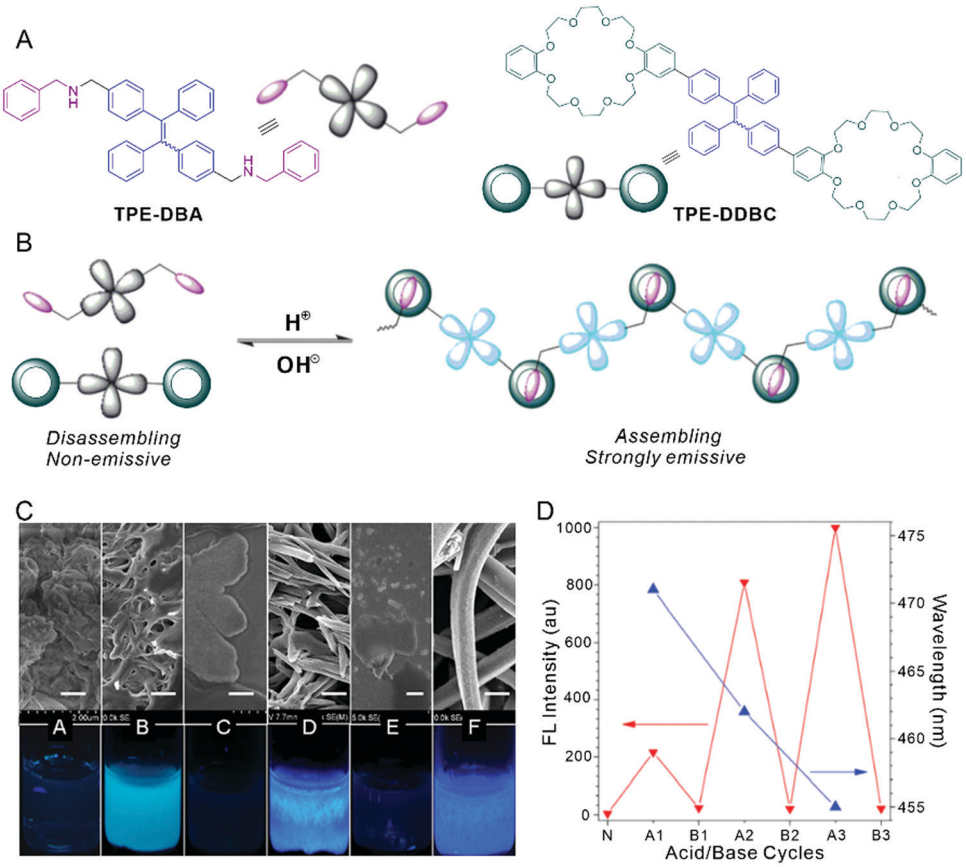

Fig. 7 Supramolecular host–guest materials based on crowns. (A) Chemical structures of the TPE-DDBC host and TPE-DBA guest. (B) Illustration of the reversible self-assembling and disassembling of host–guest complexes. (C) SEM images of the morphologies of TPE-DBA and TPE-DDBC complexes treated with HCl–NaOH solutions. (D) Plots of the changes in peak intensity and wavelength in three acid–base-treating cycles. Reproduced with permission from ref. 73. Copyright 2015 Royal Society of Chemistry.

Yan and coworkers[99] have successfully fabricated supramolecular films through the self-assembly of AIEgens, metal ions, and amphiphiles. The TPE-BPA AIEgen contains four ligands, making it strongly coordinate with metal ions to form highly charged coordinating aggregates. The subsequent combination of oppositely charged amphiphiles prohibit the coordinated aggregates to precipitate because these amphiphiles were embedded in the TPE-BPA layers that decreased their aggregating capacity, resulting in nanometer-sized, irregular coordinating clusters in water. By physically adsorbing water, these irregular coordinating clusters self-assemble into transparent macroscopic films. As these films were fabricated by electrostatic interactions, coordination, and other intermolecular interactions, the dynamic properties of intermolecular interactions rendered the supramolecular film with self-repairing and mechanical properties. Two separated films were adhered together within 10 s when pressed in a humid environment (Fig. 13A). The 3D CLSM observation revealed that the edge-to-edge welding was complete throughout the depth of the cut (Fig. 13B and C).

2.3. Macromolecular systems

Macromolecules are complexes comprising a large number of small molecules or groups linked by covalent bonds. Well-known examples are copolymers, biomolecules, DNA, and peptides. Despite the fact that intermolecular interaction is considerably weaker for smaller molecules, the collection of hundreds of small molecules largely amplifies the weak intermolecular interaction, endowing macromolecules with extremely strong intermolecular interactions and a high tendency to self-assemble into diverse supramolecular structures from micelles and vesicles to fibers and nanotubes. In addition, these macromolecular architectures usually exhibit excellent mechanical properties as a result of multiple intermolecular interactions.[100–103] Because of these outstanding advantages, macromolecules usually act as templates to guide AIEgens self-assembly into well-defined supramolecular structures. In general, AIEgens can be introduced into the side chains or backbones of polymers or incorporated into complexes to obtain AIE-containing macromolecules. In this section, several emblematic examples of AIE macromolecules will be elucidated.

One of the most popular macromolecular templates is peptides. Peptides are a type of natural macromolecules formed by several natural amino acids and possess the advantages of biocompatibility, biodegradability, and flexibility. The presence of amino acids endows peptides with a large number of hydrogen bonds, because of which peptides have become amazing

Published on 23 January 2020. Downloaded by Yunnan University on 8/9/2025 11:18:24 PM.

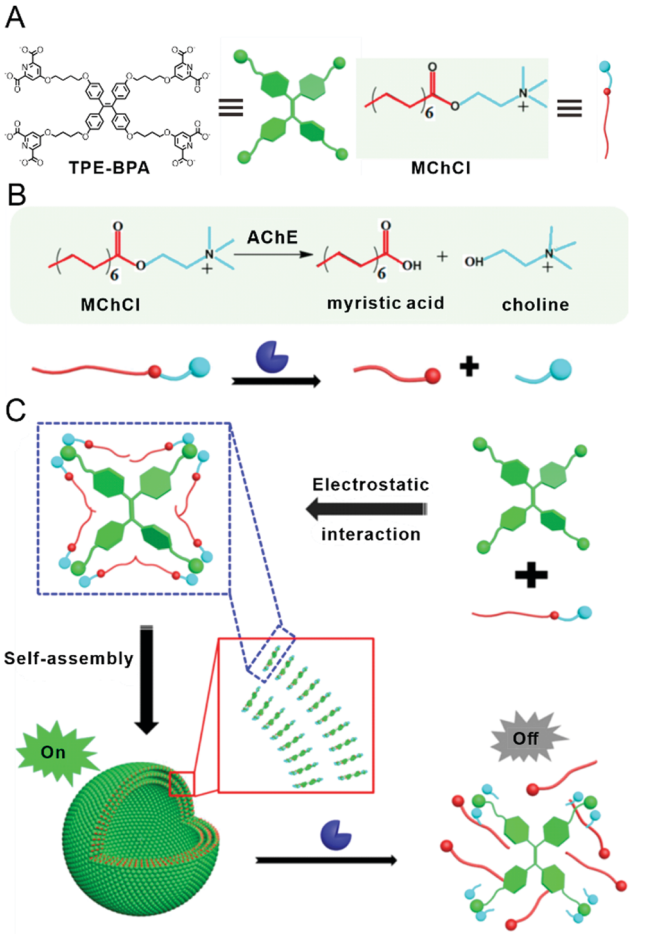

Fig. 8 Schematic illustration of the self-assembly and enzyme-linked disassembly processes of fluorescent vesicles caused by the AChE enzyme: (A) structures of TPE-BPA AIEgen and MChCl amphiphile, (B) enzymolytic reaction of MChCl, and (C) self-assembly and disassembly processes of fluorescent vesicles. Reproduced with permission from ref. 85. Copyright 2016 American Chemical Society.

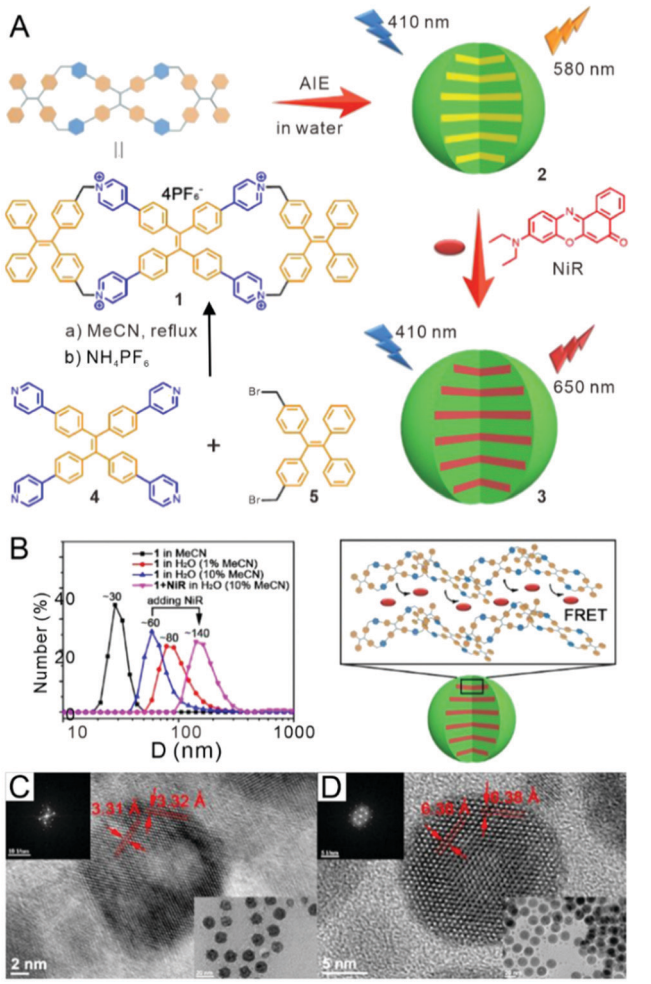

Fig. 9 Self-assembly of crystalline nanospheres. (A) Synthesis of TPE-based AIEgen and schematic illustration of AIE and light-harvesting function. (B) DLS profiles of AIEgens in solutions with different polarities, and a schematic illustration of the light-harvesting process. HRTEM images of (C) AIEgen-based nanospherical crystals and (D) Förster resonance energy transfer (FRET)-based nanospherical crystals. Reproduced with permission from ref. 87. Copyright 2019 American Chemical Society.

candidates for constructing various supramolecular materials such as fibers, vesicles, and nanotubes.[101,104–107] Exploiting the outstanding performance of peptides with regard to self-assembly, AIEgens can be combined with peptides to fabricate supramolecular luminescent materials. For instance, Liang and coworkers[108] modified the typical AIE agent, TPE, into peptide Q11 to fabricate luminescent fibers (Fig. 14A). In an aqueous solution, peptide Q11 could self-assemble into a β-sheet fibrous structure in a salt-containing environment, further entangling to form a gel network. After covalently bonding TPE on Q11 through hydrophilic amino acids, the resulting peptide Q19 dissolved in water yielding a light-blue emission. Upon increasing the concentration of NaCl salt, the emission intensity was gradually enhanced accompanied with the accumulated formation of fiber and fiber network, where TPE was encapsulated into the inner portion of the fibrous structures (Fig. 14B and C). The entrapment of TPE molecules could restrict the rotations of peripheral phenyl rings, ultimately leading to the emission enhancement of TPE. Therefore, the gelation process and evolution of fluorescence emission spectra were monitored by increasing the salt concentration.

Another prevalent macromolecular template is a block polymer, which has become a hot topic in the construction of well-defined supramolecular materials based on AIEgens. Block polymers offer superior flexibility in controlling supramolecular morphologies and functionalities by adjusting various parameters such as polymer molecular weight, building blocks, and molecular architecture, which is difficult to achieve in small-molecule systems. Therefore, block polymers have been practically applied to a wide array of fields such as nanoscale materials, drug delivery, and sensors.[109,110] Based on the diverse advantages of the self-assembly of block polymers, the polymer-templated self-assembly of AIEgens is widely used to fabricate supramolecular luminescent materials. Huang and coworkers[111] constructed multifluorescent supramolecular gels through covalently bonding AIEgens to polymers. In this work, three polymers

 This journal is © The Royal Society of Chemistry 2020

Published on 23 January 2020. Downloaded by Yunnan University on 8/9/2025 11:18:24 PM.

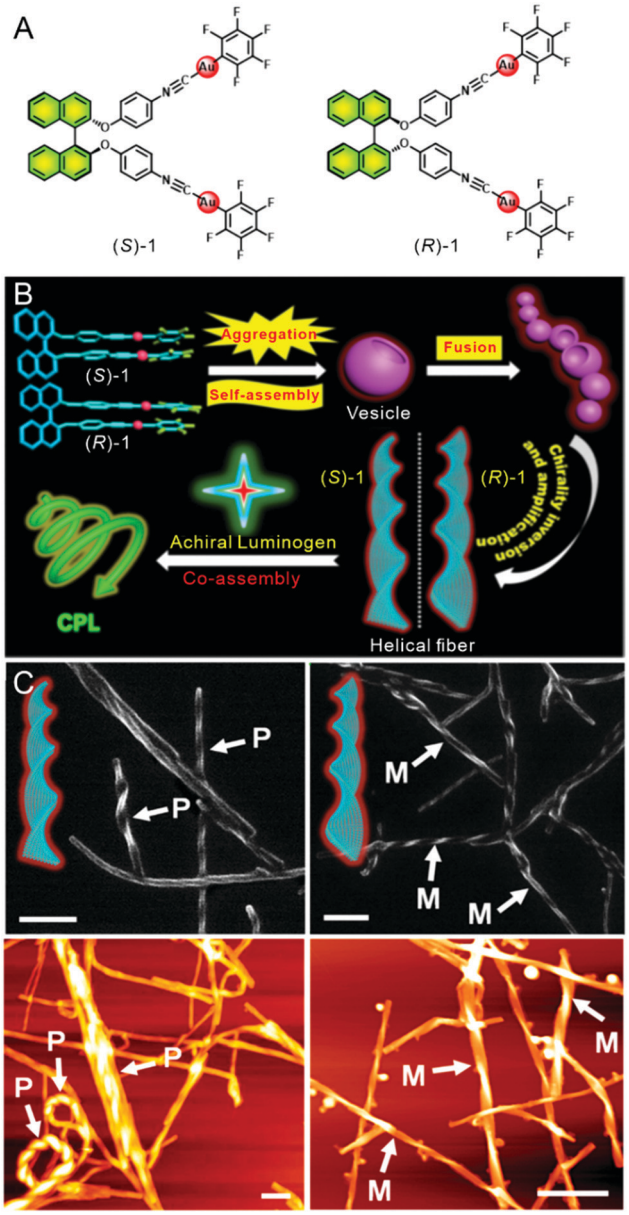

Fig. 10 Dynamic self-assembly process of helical structures. (A) Molecular structures of the chiral AIEgens (*S*)-1 and (*R*)-1. (B) Schematic representation of the hierarchical self-assembly processes. (C) SEM and AFM images of helical fibers formed by (*S*)-1 and (*R*)-1. Reproduced with permission from ref. 93. Copyright 2019 American Chemical Society.

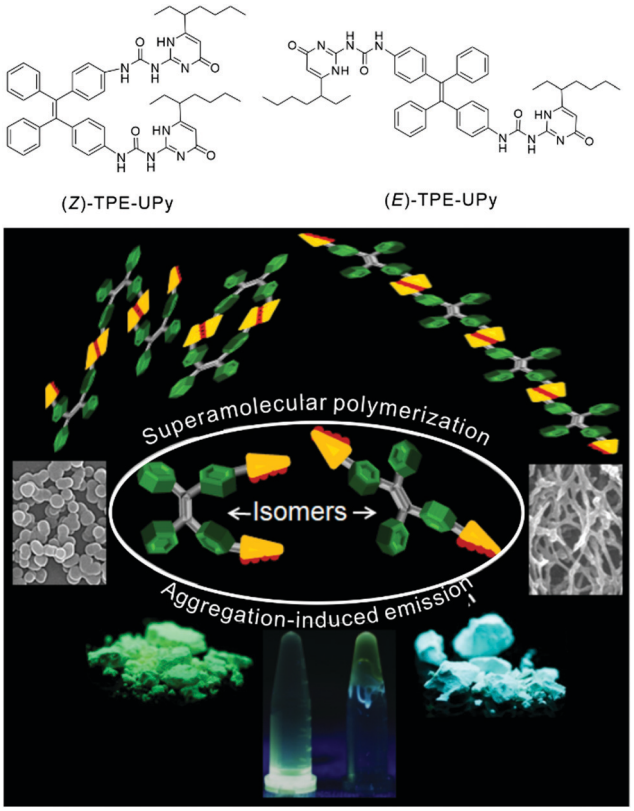

Fig. 11 Schematic illustration of the molecular structures, self-assembly processes, and fluorescence emissions of TPE-based isomers of (*Z*)-TPE–UPy and (*E*)-TPE–UPy. Reproduced with permission from ref. 97. Copyright 2017 American Chemical Society.

were fabricated by bonding three kinds of AIEgens to the side chains of UPy-containing polymers. The resulting polymers could individually self-assemble into supramolecular polymeric gels in chloroform on account of the intermolecular quadruple hydrogen bonding provided by the UPy units. Consequently, the AIEgens were restricted in the space of gels and exhibited individual yellow, blue, and green fluorescence emissions (Fig. 15A). Notably, the fluorescence emissions from the gels were tunable by mixing together two or three polymers before gel formation (Fig. 15B). This is because all the gels were formed *via* the same driving force of the UPy units. Moreover, when these discrete UPy-containing gels contacted each other, they formed an integrated supramolecular gel, where the hydrogen-bonding interactions served as the interfacial force (Fig. 15C). Further, each AIEgen in the segmented parts was independent and was not affected by the others away from the interfaces. Due to the dynamic nature and reversibility of hydrogen bonding, these gels have promising potential in the fabrication of multi-fluorescent materials with hierarchical architectures from one dimension to three dimensions.

In addition to covalent methods, noncovalent approaches can be explored for AIEgens-based polymer systems. Dynamic covalent interactions, one of the strongest noncovalent interactions, not only provide a feasible method to create supramolecular materials with complex architectures and functions, but also enable polymeric materials to have a sufficiently stable structure. Based on the well-known dynamic covalent bond of acylhydrazone, our group[112] fabricated macroscopic "Rubik's Cube" supramolecular hydrogels. These hydrogels were produced by mixing acylhydrazine-terminated polymer and tetraaldehyde-terminated polymer in water. Because of the strong structural stability and inner cavities in the hydrogels, AIEgens could be encapsulated in the hydrogels without any damage, where the rotation of AIEgens was considerably restricted. Therefore, six AIE-based hydrogels (HG-1 to HG-6) were produced and yielded six fluorescent colors upon

Published on 23 January 2020. Downloaded by Yunnan University on 8/9/2025 11:18:24 PM.

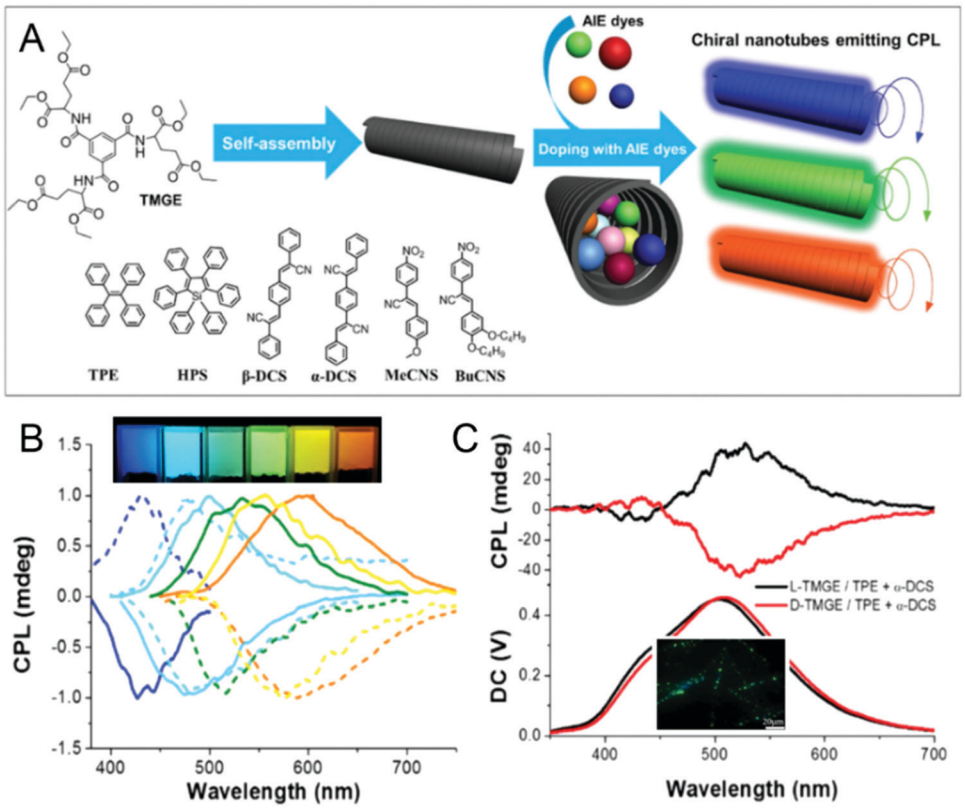

Fig. 12 Nanotube-gel-directed self-assembly of AIEgens. (A) Self-assembly process of CPL-active nanotubes through AIEgens-encapsulated TMGE gel. (B) CPL spectra of various AIEgens-encapsulated gels. Schematic representation of the hierarchical self-assembly and coassembly processes. (C) CPL spectra of a cogel made from TPE and α-DCS with TMGE excited at 363 nm. Reproduced with permission from ref. 98. Copyright 2017 Wiley-VCH.

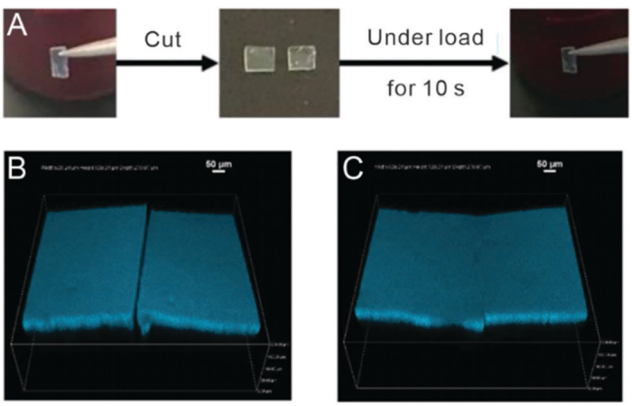

Fig. 13 Dynamic self-assembly of films. (A) Photographs of the welding of two pieces of films under a load. 3D CLSM images of the cuts on the films before (B) and after (C) edge-to-edge welding. Reproduced with permission from ref. 99. Copyright 2018 Wiley-VCH.

UV illumination (Fig. 16A). The dynamic nature of acylhydrazone bonds endowed one hydrogel to interact with another hydrogel. After exposure of the different colored hydrogels to a pre-prepared cubic hydrogel, a large percentage of the acylhydrazone bonds on the interface of the hydrogels underwent exchange and produced strong stickiness among each hydrogel, resulting in stable hydrogel tubes with six-colored faces. On the contrary, weaker interfacial interactions were exposed with shorter times (*e.g.*, 1 h) because only a small percentage of these acylhydrazone bonds were exchanged, yielding a lower level of stickiness. The strong adhesion rendered the six-colored hydrogel cubes sufficiently stable to act as building blocks, while the relatively weak adhesion made the building blocks to reversibly combine to form a Rubik's Cube and each building block could be rotated both horizontally and vertically in a concerted manner (Fig. 16B).

Moreover, the morphologies of supramolecular assemblies can be controlled in polymer systems, which facilitate the fabrication of AIEgens-based supramolecular materials with desired sizes or shapes. Until now, polymer vesicles have been successfully utilized to control the morphologies of AIEgens-based supramolecular architectures.[113,114] Polymer vesicles, namely, polymersomes, are spherical shell-like structures with a bilayer membrane made from amphiphilic block copolymers. Polymersomes with appropriate sizes and shapes are capable of entering cells for cell-compartment imaging or intracellularly releasing their cargo. Li and the coworkers[115] reported supramolecular polymersomes by TPE-functionalized amphiphilic block copolymers (TPE–PEG). The copolymers exhibited an obvious AIE characteristic: they were nonemissive when dissolved in THF or dioxane solution because the intramolecular rotation of TPE led to nonradiative decay. Upon the addition of water, fluorescence appeared and drastically increased at 99% water, which was associated with the formation of vesicular aggregates (Fig. 17A).

 This journal is © The Royal Society of Chemistry 2020

Published on 23 January 2020. Downloaded by Yunnan University on 8/9/2025 11:18:24 PM.

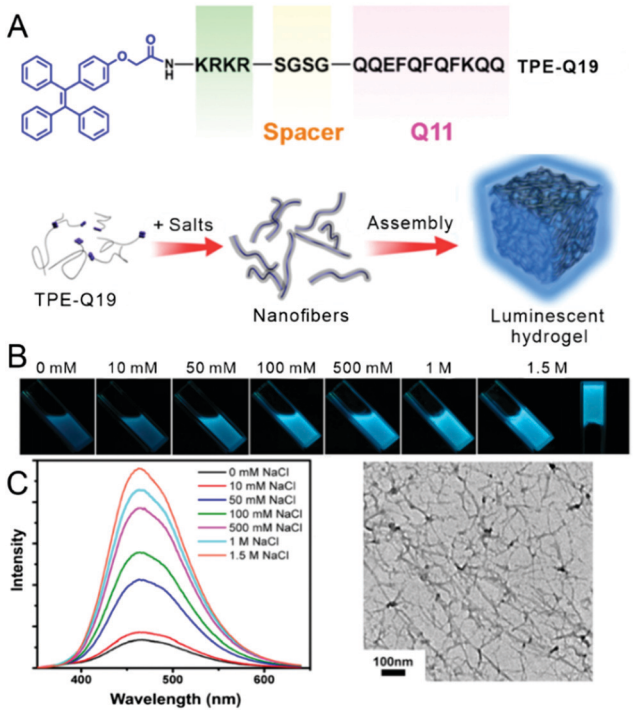

Fig. 14 Peptide-guided construction of AIEgens-based gels. (A) Chemical structures of peptides used for molecular hydrogelation, and schematic illustration of the formation of luminescent hydrogels by TPE-Q19. (B) Fluorescence images of the progressive gelation of TPE-Q19 incubated with different concentrations of NaCl. (C) Fluorescence spectra of TPE-Q19 (0.5 wt%) incubated with different concentrations of NaCl, and TEM images of TPE-Q19 gel. Reproduced with permission from ref. 108. Copyright 2014 American Chemical Society.

In these vesicles, hydrophobic TPE-containing blocks stacked with each other and self-assembled into the core of the bilayer membrane in vesicles, while hydrophilic PEG blocks were located on the surface of the membranes. Since the hydrophilic/hydrophobic ratio of the block copolymers was fairly easy to change, it was feasible to tune the aggregating ability to control the size of vesicles. Dynamic light scattering (DLS) (Fig. 17B) and TEM results (Fig. 17C) demonstrated that with a decrease in the hydrophobic block length and increase in the hydrophilic ratio, the average size of polymersomes became smaller (from 450, 250, and 90 nm to 70 nm). Yuan and coworkers[116] used TPE-containing copolymers to control the size and morphology of the fluorescent materials by changing the ratio of each component (Fig. 17D). In these copolymers, the TPE-containing blocks (BzMA–TPE) seldom dissolved in water and always formed the hydrophobic parts in the assemblies, while the hydrophilic PDMA segment was located on the interface with the aggregates. Fluorescent spherical micelles were formed in both water and alcohol solution when the polymers contained a lower percentage of BzMA–TPE blocks. The sizes of the prepared spherical micelles could also be varied by changing the length of the PDMA chain (Fig. 17E). Upon increasing the percentages of BzMA–TPE blocks, the morphologies of the assemblies transformed into worm-like micelles and vesicles. These changes were mainly driven by hydrophobic interactions. The increase in the hydrophobic parts of the polymers induced aggregates to assemble together (Fig. 17F) in order to reduce the relative hydrophilic volume and reach a stable state; further, nanostructure evolution tightened the chain packing and enhanced the confinement of AIEgens. Therefore, such a structure-correlated optical property was related to the stress variation in the core-forming chains in the aggregates. While the aggregates evolved from a small sphere to a large sphere, worm-like rods, and vesicles, the stress on the core-forming chains increased, resulting in an increase in AIE.

Moreover, polymer chains have the potential to guide the self-assembly of AIEgen-based supramolecular materials. In particular, polymers usually contain a long chain, where a large number of repeating units with binding sites are located. AIEgens can combine with these binding sites *via* covalent or noncovalent interactions and arrange through the direction of polymer chains. A typical example is the polyion assembly of the supramolecular nanoladder under the direction of the block PMVP-*b*-PEO polyelectrolyte (Fig. 18A).[117] In this work, the properly shaped TPE derivates (TPE-C4-L2) showed negligible fluorescence and no aggregates were formed in water. The coordination with zinc ions slightly increased fluorescence emissions, and the aggregates were formed with flat and cocoon-like sheets. After the further addition of positively charged PMVP-*b*-PEO, the polydisperse cocoons immediately transformed into uniform nanoladders (Fig. 18B–D). In these nanoladders, negatively charged coordination complexes bonded to the positive PMVP block and arranged in a highly ordered manner along the positive chains, where each chain aligned parallelly to each other, thereby generating a grid-like structure. The PEO blocks formed a very thin layer, which was surrounded by the ladders and provided steric repulsions to prevent the ladders from bundling. Most importantly, the fully extended chain of PMVP determined the width of the nanoladders. Using a similar strategy, Yang's group[118] presented a hierarchical self-assembly of pearl-necklace-like networks guided by a natural polymer, heparin (Fig. 18E). Owing to the presence of carboxylate groups and sulfate in the main chains, linear and unbranched heparin possessed a highly negative charge density. As a result, heparin could combine positively charged molecules or complexes through electrostatic interactions to form well-defined supramolecular architectures. TPE-containing dipyridine coordinated with diplatinum(II) acceptors to form metallacycle complexes. These metallacycles carried a highly positive charge, which enabled them to combine with heparin and orient along the long chain of heparin. The flexible chain of heparin further intertwined into entangled 3D pearl-necklace-like networks.

3. Applications of AIEgens-based supramolecular materials

In principle, the AIE effect endows supramolecular materials with excellent fluorescence abilities, which not only improves the functional performances, but also creates new applications in a large range of fields.[119–122] Because of worldwide efforts,

Published on 23 January 2020. Downloaded by Yunnan University on 8/9/2025 11:18:24 PM.

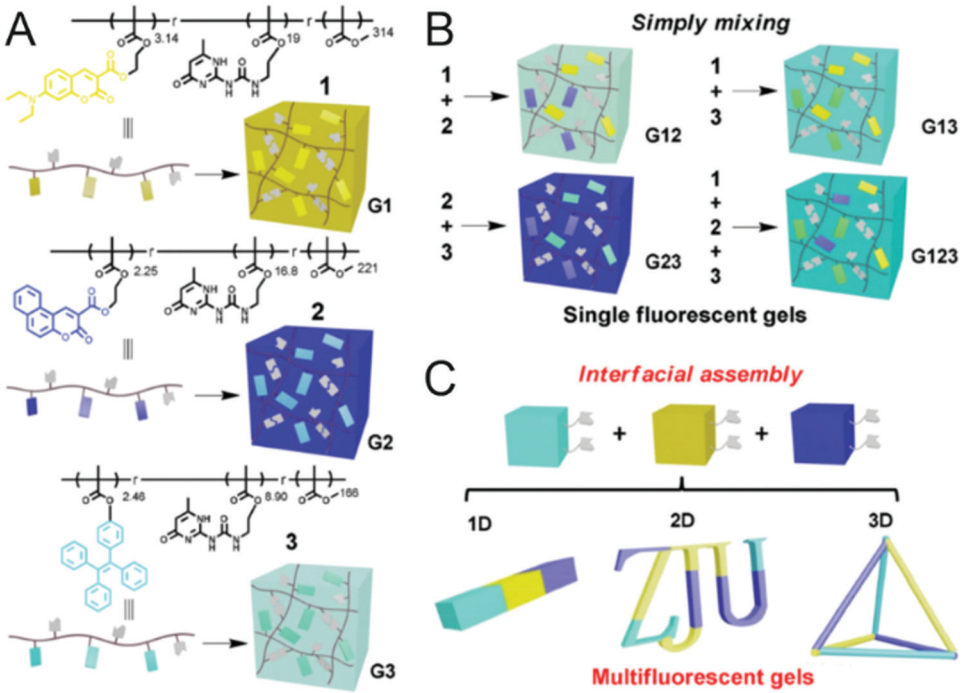

Fig. 15 Polymer-guided construction of AIEgens-based gels. (A) Chemical structures of three AIEgens-containing polymers 1, 2, and 3, and schematic representations of G1, G2, and G3. (B) Schematic representations of G12, G13, G23, and G123. (C) Schematic representations of multifluorescent polymeric gels constructed from discrete fluorescent gels (G1, G2, and G3) *via* multiple hydrogen-bonding interactions at the interfaces. Reproduced with permission from ref. 111. Copyright 2015 Wiley-VCH.

many AIEgens-based supramolecular materials have been developed, and their applications have been elaborately explored. In this section, we summarize the recent applications of AIEgen-based supramolecular materials in different fields.

3.1. Sensors

The construction of AIEgens-based supramolecular fluorescent materials usually involves noncovalent interactions, such as hydrophobic effect, electrostatic interaction, and host–guest interaction. As these noncovalent interactions are relatively weak and dynamic, supramolecular materials are always reversible in structure, where only a low energy is required to disrupt or reconstruct the supramolecular architecture. Therefore, external stimuli usually trigger supramolecular materials to undergo a structural change or destruction. Meanwhile, the AIEgens in supramolecular materials alter their packing states during the rearrangement process of structures or morphologies, resulting in an increase or decrease in fluorescence emissions. The fluorescence emission variations upon external stimuli enable AIEgen-based supramolecular materials to be utilized as sensors in various fields. Until now, various fluorescent supramolecular materials based on AIEgens have been developed to detect diverse biomolecules such as proteins, enzymes, genes, and inorganic ions.

Several "turn-on" fluorescence sensors based on AIE-based supramolecular materials have been developed for the detection of biomolecules. The "turn-on" emission originates from the biomolecule-induced self-assembly of the dispersed AIEgens. In particular, the dispersed AIEgens are always nonemissive. After the combination with specific molecules, such as a biomarker through intermolecular interactions, AIEgens could self-assemble into supramolecular complexes and exhibit strong emissions due to the restriction of the intermolecular rotation of AIEgens. The highly sensitive fluorescence "turn-on" capacity enables AIEgens to perform as excellent sensors. Heparin is an important biomolecule, which is relevant to the regulation of blood coagulation, immune response, and cell growth. In addition, heparin also serves as a carbohydrate drug and anticoagulant in clinic. Lee's group[123] prepared a fluorescent "turn-on" peptide-modified TPE probe to detect heparin. The presented AIE probe was prepared to detect heparin. This AIE probe selectively combined with heparin through electrostatic interactions, and it further self-assembled into supramolecular nanoparticles. Here, the TPE segments were located in the core of the nanoparticle, and their molecular rotations were restricted, resulting in strong emissions at 475 nm. This "turn-on" fluorescence response to heparin was highly sensitive with a limit of detection (LOD) of 138.0 pM in water and 2.6 nM in serum samples. Similarly, Ding's group[124] reported a highly sensitive TPE-GFFYK(DEVDEE-Ac) probe by the incorporation of two peptide sequences to AIEgens for detecting caspase-3—an enzyme that plays significant roles in mediating cell apoptosis. Owing to the hydrophilicity of the DEVD peptide sequence, this probe showed excellent solubility and was nonemissive in water. In the presence of caspase-3, the carboxylic group of hydrophilic DEVD was cleaved; therefore, the self-assembling GFFY peptide sequence guided the hydrophobic TPE residues to form well-defined fibers. The TPE groups exhibited highly ordered packing

 This journal is © The Royal Society of Chemistry 2020

Published on 23 January 2020. Downloaded by Yunnan University on 8/9/2025 11:18:24 PM.

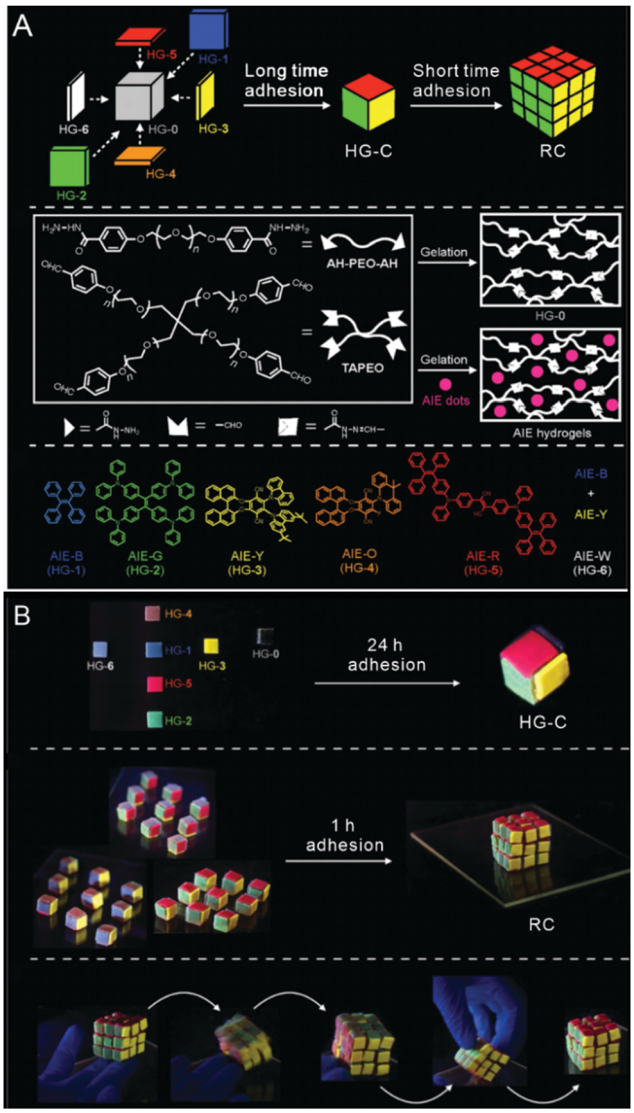

Fig. 16 AIEgens-based gels constructed *via* noncovalent interactions. (A) Schematic showing the preparation of a chemical Rubik's Cube (RC) through the macroscopic adhesion of HG-0 hydrogel and AIE-based hydrogels, and the chemical structures of hydrogels and AIEgens. (B) Photographs showing the formation of the building block (HG-C hydrogel) *via* the macroscopic adhesion of HG-0 hydrogel and AIE-based hydrogels, the formation of a Rubik's Cube-like hydrogel through the macroscopic adhesion of individual HG-C hydrogel blocks, and hydrogel RC being rolled by hand. Reproduced with permission from ref. 112. Copyright 2019 Wiley-VCH.

in the fibers, where their intramolecular rotations were considerably restricted and exhibited obvious turn-on fluorescence. This probe had ultrahigh sensitivity toward detecting caspase-3 in water with LOD of 0.54 pM, and it could also be utilized in a cellular environment.

In addition to the combination with analytes, fluorescence could also occur due to the disruption of AIEgens-based supramolecular materials. Our group[125] reported another "turn-on" sensor based on supramolecular materials to detect α-amylase. In an aqueous solution, hydrophobic TPE was encapsulated in the cavity of γ-CD *via* a host–guest interaction. No emission signal was observed mainly because the phenyl rings of TPE could freely rotate in the large-sized cavities of γ-CD. When γ-CD was hydrolyzed by amylase, the TPE residues were released from the cavities and a large number of aggregates were formed in the water driven by the hydrophobic interaction. As a result, the fluorescence was obviously enhanced due to the restriction of rotation in the TPE aggregates. Because of the distinct "turn-on" signals, this sensor showed excellent sensitivity to α-amylase with LOD of 0.007 μm L^{-1}.

A color-variation strategy based on the FRET effect could also be adopted in AIEgen-based supramolecular sensors for sensing biomolecules. Generally, a FRET system is a complex system comprising a donor fluorescent molecule and an acceptor fluorescent molecule, where the emission from the donor acts as the excitation for the acceptor. Tian and coworkers[126] fabricated a FRET sensor to detect both amyloid β (Aβ) and lectins. The FRET sensor was constructed by simply mixing glycol probes and AIEgen-based DES in an aqueous buffer solution *via* hydrophobic interactions. AIEgen-based DES emitted green fluorescence in water and acted as the donor, while the FRET system yielded a red emission and worked as the acceptor. Therefore, upon the excitation of DES, these sensors produced a red emission at 620 nm. In the presence of Aβ, the emission of sensors varied from red to orange peaking at 525 nm; this is because the specific interaction between hydrophobic DES and the hydrophobic region of Aβ increased the distance between the donors and acceptors, consequently changing the FRET efficiency. Since Aβ is a well-established biomarker for Alzheimer's disease (AD), these sensors could be efficiently used for AD diagnosis. When lectins were added into the FRET system, the emission color changed to green at 490 nm, because the glycosyl moiety of the glycol probes selectively and competitively interacted with the lectins to form nanoparticles, leading to the breakdown of FRET systems.

Moreover, the "turn-off" feature provided another strategy for AIEgens-based supramolecular materials to be used in the field of biomolecule detection. In the disassembly process of supramolecular materials, the AIEgens generally underwent a transformation from an intense arrangement to the dispersed state, where the restriction of molecular motion is absent, resulting in the disappearance of fluorescence. Liang and coworker[127] fabricated a "turn-off" fluorescence sensor based on the self-assembled nanoparticles of negatively charged hyaluronic acid (HA) and quaternary-ammonium-modified TPE derivative. In water, the self-assembled nanoparticles efficiently emitted blue fluorescence with a quantum yield of 6.38%. The addition of hyaluronidases (HAase) induced a time-dependent decrease in the fluorescence intensity, while the fluorescence seldom changed in other enzymatic systems, benefiting from the specific enzymatic reaction between HAase and HA. This obvious change in fluorescence could be used to selectively detect HAase.

In addition to sensing biomolecules, AIEgens-based supramolecular materials played an important role in detecting inorganic compounds. Zinc ions play an essential role in the biological processes of plants, animals, and human beings, such as signal transduction and metabolism of DNA and RNA.

Published on 23 January 2020. Downloaded by Yunnan University on 8/9/2025 11:18:24 PM.

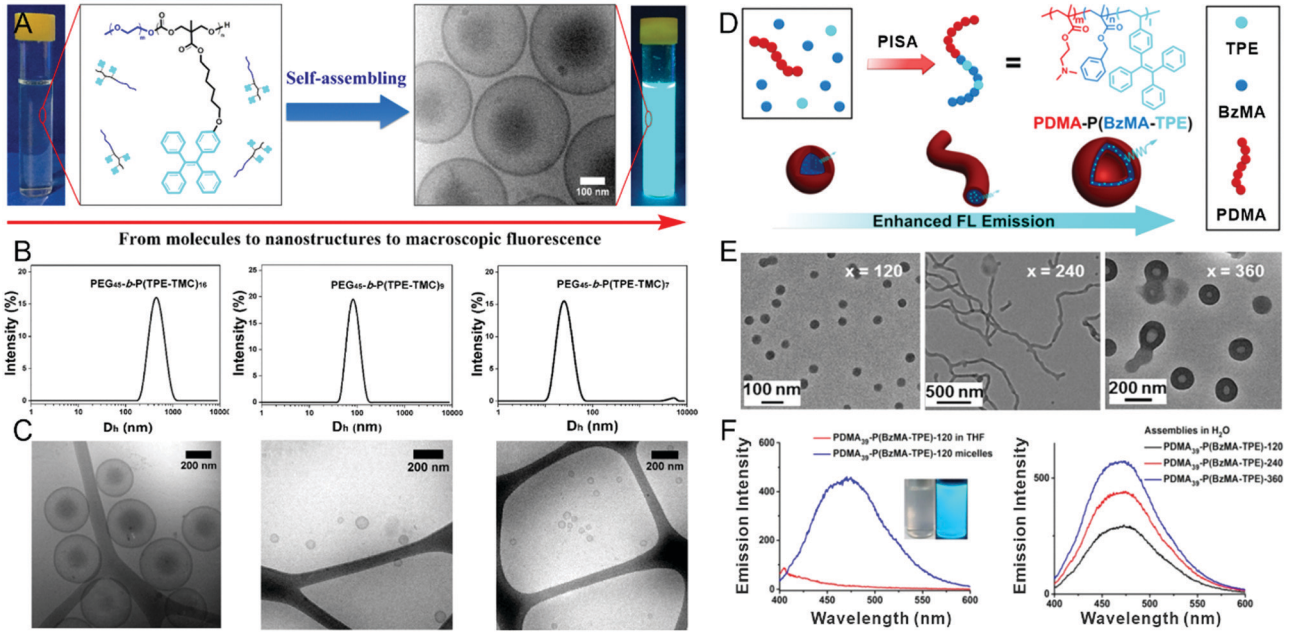

Fig. 17 Size and morphology control in AIEgens-based supramolecular assemblies. (A) Self-assembly of AIEgens-based polymersomes. (B) Size distribution and (C) cryo-TEM images of polymersomes for polymers with different PEG fractions. Reproduced with permission from ref. 115. Copyright 2018 American Chemical Society. (D) Schematic representation of the preparation of AIE-based assemblies. (E) Morphological characterization and (F) AIE effect of AIE-based assemblies with different dispersion polymerizations of BzMA and TPE. Reproduced with permission from ref. 116. Copyright 2017 American Chemical Society.

Many diseases including AD, epilepsy, and ischemic strokes are relevant to the abnormal expression of zinc ions in the pathological processes. Jung's group[128] reported a turn-on chemoprobe for Zn^{2+} detection based on benzene-1,3,5-tricarbozamide-appended terpyridine ligand (BT_3). The ligand self-assembled into nanofibrous structures in DMSO/H_2O solution, but it showed weak emissions because of the formation of H-aggregation, where the strong π–π stacking between the terpyridine groups of BT_3 caused emission quenching. Upon coordination with Zn^{2+}, the terpyridine groups changed their molecular configurations into the horizontal direction, resulting in the degradation of π–π stacking. The coordinated complexes self-assembled into spherical nanoparticles through the hydrogen bond between the amide and amide groups. The intramolecular rotations of BT_3 were restricted in the coordinated complex, thereby yielding strong fluorescence emissions.

Macrocycles and their derivatives have been widely explored as sensors to detect inorganic compounds because of their favorable recognition toward various types of inorganic guest molecules. For instance, Yang's group[129] utilized pillar[5]arene-containing conjugated macrocycle polymer (CMP) to construct fluorescence sensors to selectively detect metal ions. In the CMP, ditriflate-functionalized pillar[5]arene and TPE cores were covalently connected *via* an extremely short ethyne spacer (Fig. 19A). As a result, the intermolecular rotation of TPE was considerably restricted, leading to enhanced fluorescence from the CMP material. Due to the excellent specificity of the methoxy group and size-matching effect of pillar[5] toward ferric ions, the fluorescence was remarkably quenched only in the presence of ferric ions (Fig. 19B), allowing CMP to act as the selective sensor toward Fe^{3+}. Moreover, this pillar[5]arene-based CMP showed high sensitivity and selectivity in the detection of 4-amino azobenzene—a carcinogenic dye—by the way of luminescence quenching. Recently, Yang's group[130] fabricated a supramolecular macrocycle system to efficiently detect mercury(II). Mercury(II) is indeed a serious threat to human beings because it can severely damage the immune system, kidneys, and central nervous system. The employed macrocycle system was fabricated by self-assembling thymine (T)-modified pillar[6]arene (H) and quaternary ammonium (G)-bonded AIEgens TPE derivate. Due to the host–guest interaction between H and TPE-bridged guest (G), supramolecular complexes were formed, but they exhibited negligible fluorescence emissions. The intermolecular interaction in the complex was very weak such that the TPE segment could freely rotate and release the energy in a nonradiative manner. However, the fluorescence emission was remarkably increased upon the addition of Hg^{2+} because the tight covalent bonding between Hg^{2+} and thymine, *i.e.*, T–Hg^{2+}–T bonds, induced the formation of highly intensive and compacted spherical-like supramolecular nanoparticles (Fig. 19C). This enabled the supramolecular complexes to serve as a sensor and absorber for Hg^{2+}. Significantly, Hg^{2+} could be continuously removed, and the supramolecular complexes could be regenerated by the simple addition of Na_2S (Fig. 19D). Therefore, AIEgen-based supramolecular materials played the dual role of selective detector and remover of toxic Hg^{2+}.

3.2. Nanomedicine

In traditional fluorescent–molecule systems, the ACQ effect yields supramolecular materials with negligible emissions.

 This journal is © The Royal Society of Chemistry 2020

Published on 23 January 2020. Downloaded by Yunnan University on 8/9/2025 11:18:24 PM.

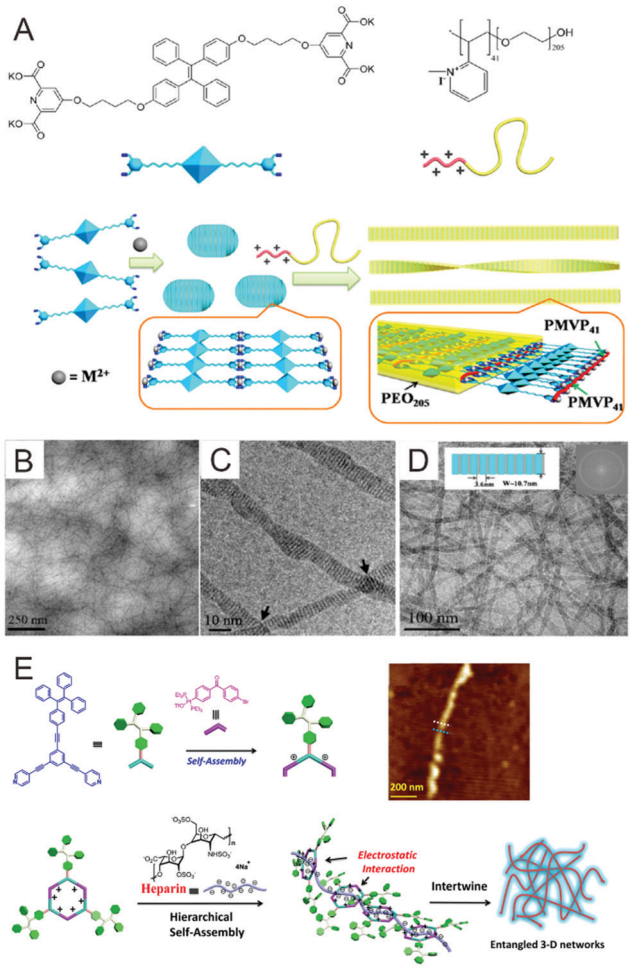

Fig. 18 Polymer-directed construction of AIEgens-based fibers. (A) Schematic representation of the construction of nanoladders by TPE-C4-L2 and metal ions and with polymers. (B–D) Cryo-TEM images of the nanoladders at different magnifications. Reproduced with permission from ref. 117. Copyright 2015 American Chemical Society. (E) Formation process of 3D networks by TPE-containing metallacycle and heparin. Reproduced with permission from ref. 118. Copyright 2014 American Chemical Society.

On the contrary, AIEgens exhibit extremely obvious fluorescence in well-defined morphologies such as vesicles, micelles, nanotubes, and nanoribbons because the intermolecular interactions are intensely restricted in the highly ordered arrangement and energy relaxation occurs radiatively. In addition to high signal-to-noise ratios, AIEgen-based supramolecular materials possess the advantages of high photobleaching threshold and large Stokes shift. These impressive advantages allow AIEgens-based supramolecular materials to act as excellent imaging agents to visualize *in vitro* and *in vivo* therapeutic performances.

Liang and coworkers[131] fabricated fluorescent nanofibers through the supramolecular self-assembly of TPE-labeled short peptide TR4 with plasmid DNA. Based on the hydrophobic agents and positively charged arginine agents of TR4, positively charged plasmid DNA combines with TR4 to form complexes and further self-assemble into supramolecular fibers (Fig. 20A and B). The hydrophobic TPE moieties were intensely stacked and aggregated in the inner area of the fibers, where the intramolecular rotation of TPE was considerably restricted, thereby exhibiting an obvious blue emission in water and displaying self-indicating properties for tracing the gene delivery process *in vitro* (Fig. 20C and D). TPE-labeled TR4 molecules could also specifically combine with positively charged siRNA to form supramolecular spherical nanoparticles.[132] The surface of supramolecular nanoparticles was further coated with proteins for targeting cancer cells. As the moist TPE was intensely assembled in the core of the nanoparticles, these nanoparticles exhibited a strong blue emission. This strong emission clearly revealed the process of entering the cells, revealing that proteins could accelerate the release of siRNA into cytosol and therefore achieving higher gene-silencing efficiency.

Wu and coworkers[133] demonstrated a facile strategy to trace intracellular anticancer drug delivery *via* the synergetic combination of AIE effects and FRET. The anticancer drug, DOX, was encapsulated into polymeric micelles in an aqueous solution self-assembled by an amphiphilic polymer, PEG–POSS–$(TPE)_7$. These polymeric micelles having blue emissions exhibited AIE features originating from the aggregated TPE units *via* Schiff base bonds, which were strengthened by restricting the intramolecular rotations of TPE units through the incorporation of rigid cage-shaped POSS groups. After the encapsulation of DOX into these micelles, an efficient FRET system was established between the TPE donors and DOX acceptors, resulting in strong red luminescence emitted from the micelles instead of blue luminescence within the cells, thereby exhibiting better self-localized properties. After rapid endocytosis, the micelles thoroughly and quickly released DOX with red emissions under acidic environments in the endosome/lysosome because of the protonation of the Schiff base, yielding a blue emission again. The different emission colors from the micelles and DOX could clearly localize them within the cells; therefore, the subsequent escape of the released DOX from the endosome/lysosome to the nucleus in the cells could be observed.

Near-infrared (NIR) fluorescent materials have attracted increased attention in the recent years and have been widely used in biological applications because of the impressive advantages of NIR fluorescence emissions (650–900 nm), such as slight photodamage on biological systems, deep tissue penetration, and minimum background interference from biomolecule autofluorescence. A large number of NIR AIEgens have been formulated in the recent years based on the strategies of extending conjugated systems or electron-donating and electron-accepting (D–A) molecular engineering.[134–139] These NIR AIEgens provide a series of opportunities to construct supramolecular NIR fluorescent materials. For instance, Gao and his groups[140] developed supramolecular nanoparticles with high NIR emission and mitochondria-targeting ability based on AIEgen-containing polymers. In such AIEgens, diphenylamine acted as the electron-donating segment, while cyano was used as the electron-withdrawing group to ensure NIR emissions. The steric hindrance between the two groups twisted their conformation to result in AIE characteristics. The AIEgen, associated with hydrophilic triphenylphosphine groups, was covalently

Published on 23 January 2020. Downloaded by Yunnan University on 8/9/2025 11:18:24 PM.

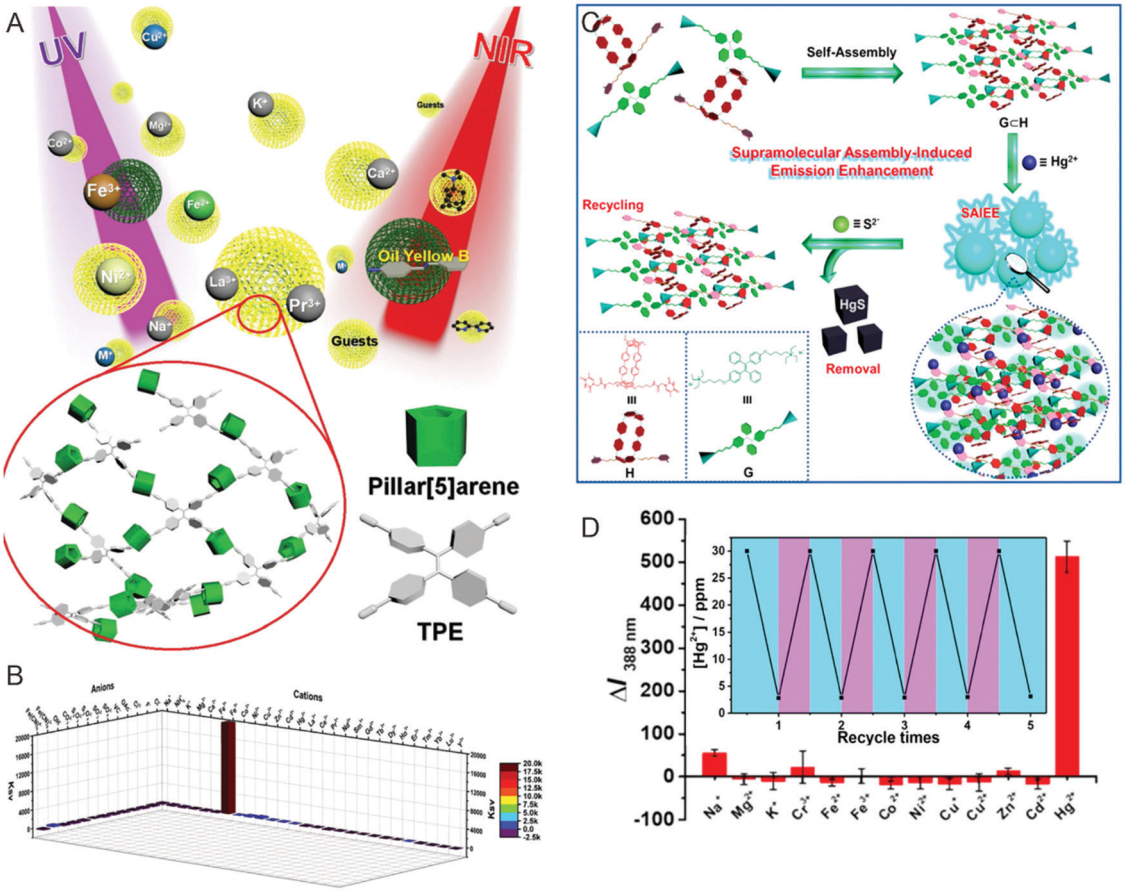

Fig. 19 AIEgen-based sensors for the detection of metal ions. (A) Schematic representation of conjugated macrocycle polymer based on pillararene and TPE and (B) its selective sensing to ferric ions. Reproduced with permission from ref. 129. Copyright 2018 Wiley-VCH. (C) Schematic illustration of the sensing and removal of Hg^{2+} from water based on the "switch-on" fluorescence of the supramolecular polymers and (D) the regeneration–recycling process. Reproduced with permission from ref. 130. Copyright 2019 American Chemical Society.

linked to the side chains of polyethylene glycol (PEG). In aqueous media, this polymer self-assembled into spherical nanoparticles (size: ~260 nm) and exhibited a fluorescence quantum yield of 3.6%. Because of the mitochondria-targeting function of triphenylphosphine groups, the nanoparticles could be specifically enriched in the mitochondria of cells, yielding excellent imaging performance. Moreover, two-photon fluorescence probes could be excited by NIR or infrared wavelengths, showing promising potential in bioimaging. The development of two-photon fluorescence probes with AIE features has been a new topic in accurate tumor diagnoses.[141–143] Wang and coworkers[144] covalently bonded two-photon AIE molecules to a copolymer to prepare redox and pH dual-responsive supramolecular micelles. The excitation wavelength of these micelles was 410 nm. The emission from these micelles could also be excited by an 800 nm laser, yielding an obvious red color. The cellular uptake of micelles, AIE-active cell, and tissue imaging were evaluated under the irradiation of an 800 nm laser.

External stimuli usually trigger morphological changes or structural destruction of supramolecular materials, where AIEgens vary their arrangement and aggregation degrees. As a result, the brightness or colors of emission are drastically changed. This endows supramolecular materials with promising potential in therapy by targeting selectively releasing loaded drugs to treat diseases. The integration of diagnosis and therapeutics into one platform could simultaneously achieve the detection of diseases, monitoring drug distribution, and evaluation of therapeutic effects, which has become one of the most promising technologies in the field of nanomedicine. For instance, Sessler and coworkers[145] recently reported pH-responsive fluorescent vesicles to monitor the release of the loaded drugs. These vesicles were fabricated by the host–guest complexes of calix[4]pyrroles and TPE derivate. Calix[4]pyrroles are macrocycles consisting of four pyrrole units linked with carboxylates, which allowed TPE-containing pyridine *N*-oxide derivatives to be deeply embedded within their aromatic cavities. TPE groups were stacked in a highly ordered arrangement in the vesicle membrane, yielding strong emissions due to the fact that the rotation of phenyl rings of TPE was restricted. Upon exposure to acidic conditions, calix[4]pyrroles underwent protonation and formed small solid nanoparticles, where the TPE derivatives were released from the cavities. The solution showed extremely weak emissions because the TPE-containing derivatives were effectively dissolved in water, and the phenyl rings could

 This journal is © The Royal Society of Chemistry 2020

Published on 23 January 2020. Downloaded by Yunnan University on 8/9/2025 11:18:24 PM.

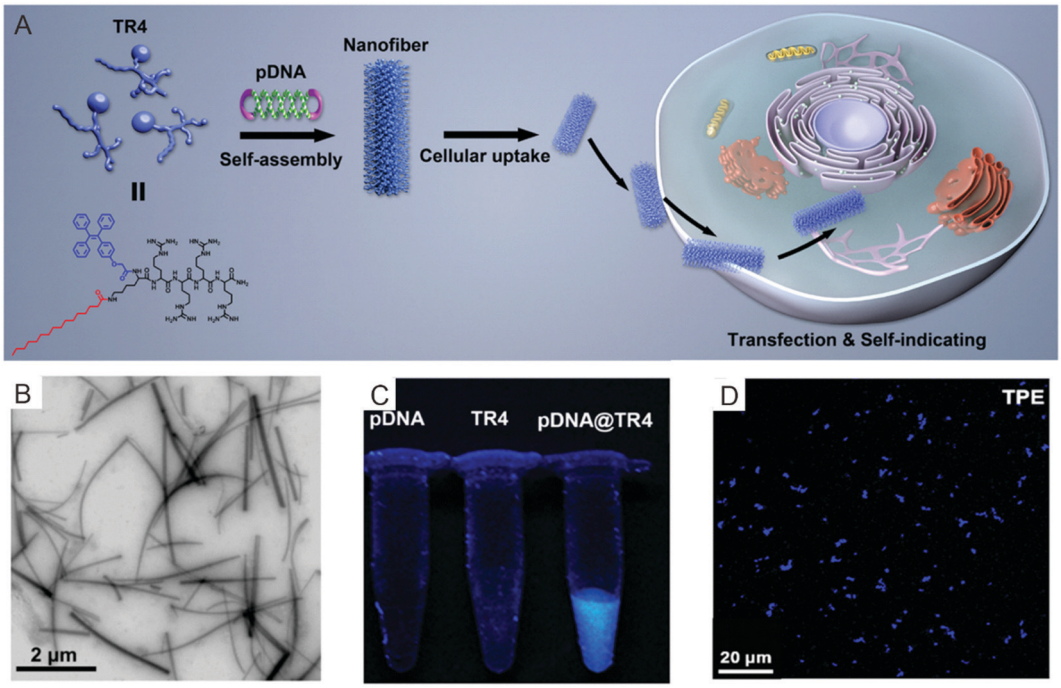

Fig. 20 AIEgen-based supramolecular materials for imaging. (A) Schematic illustration of the formation and transfection of AIE nanofibers constructed from TR4 and plasmid DNA for traceable gene delivery. (B) TEM, (C) fluorescence, and (D) CLSM images of DNA@TR4 complexes. Reproduced with permission from ref. 131. Copyright 2017 American Chemical Society.

rotate freely. Since the morphological variation from self-assembled vesicles to small solid nanoparticles was associated with the disappearance of fluorescence, this intrinsic difference in fluorescence was used to detect the release of nonemissive loaded molecules.

The discovery of photodynamic therapy (PDT) using AIE-active photosensitizers has prompted their applications in theranostics. In general, the radiative dissipation from the singlet excited states to the ground state results in fluorescence emissions. Alternatively, the exciton can undergo the intersystem crossing (ISC) process to form the triplet excited states, producing ROS, such as radicals and singlet species ($^1O_2$), upon reacting with the surrounding molecules or oxygen. These cytotoxic ROS can kill cancer cells.[146,147] However, ACQ effects cause conventional photosensitizers to have extremely low efficiencies with regard to fluorescence emission and ROS production, making the use of conventional photosensitizers as multifunctional supramolecular materials to become challenging. Benefiting from the tremendous development of AIEgens, many AIE-based photosensitizers have been elegantly designed and presented, which have successfully overcome these obstacles. In the highly ordered state of supramolecular materials, AIEgens largely block the nonradiative pathway and promote both the radiative pathway and ISC process. As a consequence, AIE-based photosensitizers not only provide distinguishable emission from the visible to NIR regions, but also exhibit excellent photosensitizing ability. Therefore, AIE-based supramolecular materials can be applicable for imaging and therapeutic functions without necessitating clinical drugs. For example, Liu's group[148] developed a light-controlled gene delivery system based on an AIE-based photosensitizer. This delivery system was fabricated through the self-assembly of DNA and copolymers (Fig. 21A), which contained AIEgens-conjugated OEI *via* aminoacrylate (AA) linkers and PEG blocks. OEI conjugates carried high charges and therefore had good DNA-binding ability, which enabled the copolymer to combine with DNA and further self-assemble into supramolecular nanoparticles in aqueous solutions (Fig. 21B). Therefore, the AIEgens were intensely packed and showed bright red fluorescence, thereby rendering nanoparticles with excellent performance for bioimaging applications. Upon light irradiation, the generated ROS disrupted the membranes of lysosomes, facilitating the nanoparticles to escape from the lysosomes. Meanwhile, the ROS also decomposed the polymer into its low-molecular-weight counterparts, leading to the release of DNA for efficient gene therapy (Fig. 21C). Recently, Liu and coworkers[149] prepared a vesicle with both imaging and PDT functionalities by incorporating AIEgens into lipids (Fig. 22). These AIEgens were anchored inside the bilayer of the membranes and exhibited intrinsic bright red fluorescence due to the restriction of molecular motion. The strong emission could be used to clearly monitor the cellular uptake process and the distribution of AIEsomes, where the vesicles were located from the membrane to the endosomes and lysosomes of the cells. Meanwhile, the AIEgens endowed the photosensitization ability to the vesicles, which showed efficient ROS generation and played a vital role in killing cancer cells. Significantly, the ROS-generating efficiency was related to the morphology of supramolecular materials. AIEsomes exhibited better ROS-generating efficiency than nanospheres containing the same concentration of AIEgens. It seems reasonable to infer that the higher surface area of AIEsomes and

Published on 23 January 2020. Downloaded by Yunnan University on 8/9/2025 11:18:24 PM.

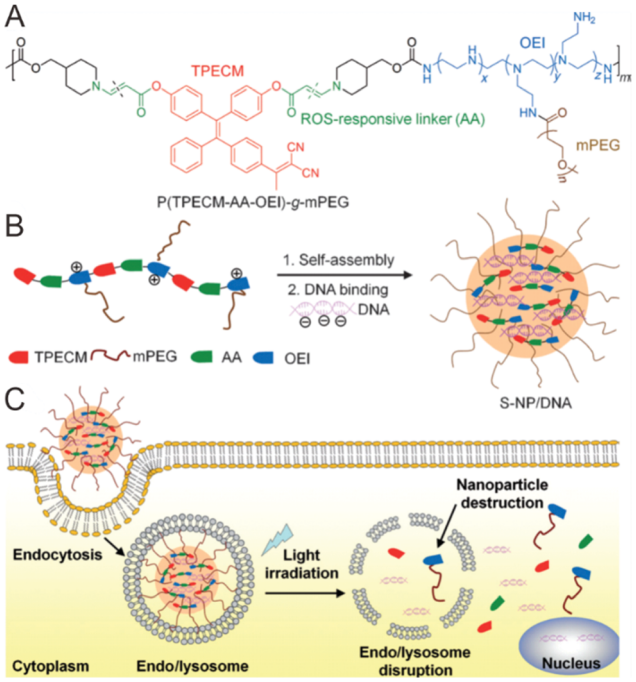

Fig. 21 AIEgens-based delivery with the PDT effect. (A) Chemical structures of the ROS-responsive and AIEgens-containing polymers. (B) Self-assembly of ROS-sensitive nanoparticles in aqueous media and their complexation with DNA. (C) Itinerary of DNA-loaded nanoparticles to the transgene expression. Reproduced with permission from ref. 148. Copyright 2015 Wiley-VCH.

looser packing of AIEgens could induce better oxygen diffusion inside the thin lipid bilayer, while AIEgens inside the NPs formed large solid aggregates such that the photosensitizers located inside the deep core were hardly exposed to free oxygen.

3.3. Visualization

Constructing supramolecular materials always involves the spontaneous self-assembly process from small molecules to large-scale aggregates, which is often associated with morphological transformation. Investigating the self-assembly processes offers a fundamental understanding of the structure-related properties of supramolecular materials. Fluorescence, which has been proven to be a fairly sensitive and easily accessible technique, allows a series of opportunities to visualize the real-time self-assembly process. However, the formation or transition of supramolecular materials occurs in the aggregated or solid states, respectively, and the visualization of these processes is severely inhibited by the ACQ effect of conventional fluorophores. The discovery of AIEgens remarkably promotes the development of luminescent materials by overcoming the ACQ effect. Because of the highly efficient emission from the aggregated states of AIEgens, numerous self-assembly processes have been successfully observed.

Micelles are the ordered assemblies of amphiphiles with sphere-, rod-, or worm-like structures. They are generally formed when the amphiphile concentration is higher than the critical micelle concentration (CMC).[150–152] Taking advantage of the intense fluorescence emission of AIEgens in the aggregated state, the formation process of micelles, as well as the

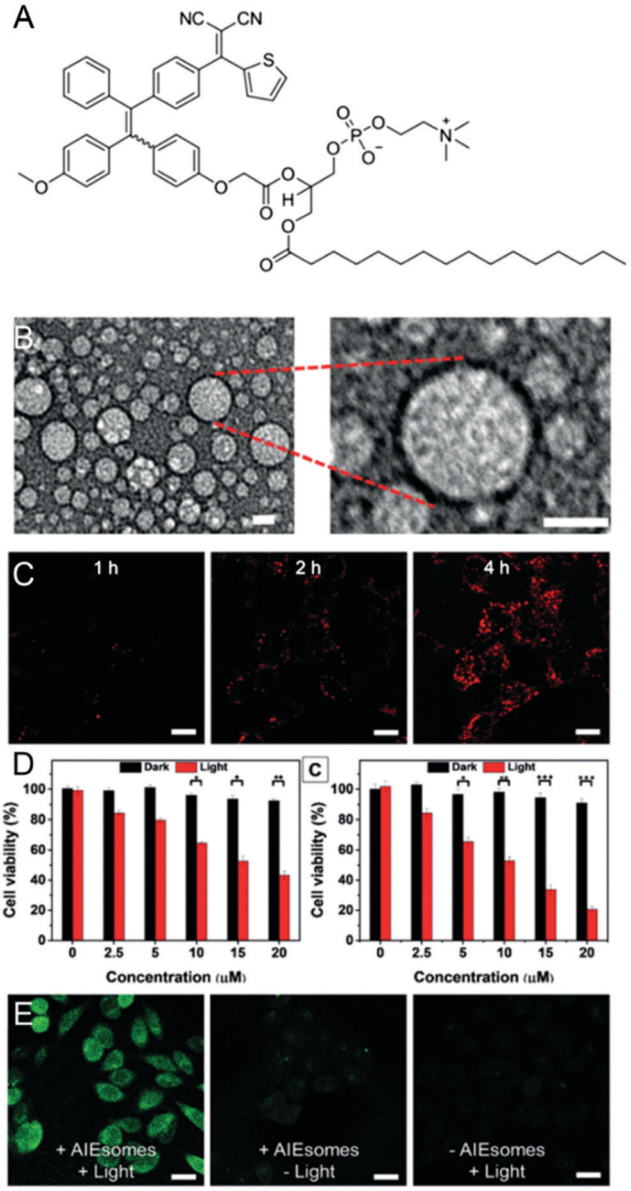

Fig. 22 AIEgen-based liposomes with the PDT effect. (A) Chemical structure of the AIEgen–lipid molecule. (B) TEM image of AIEsomes. (C) CLSM images of live 4T1 cancer cells after incubation with AIEsomes for different times. (D) 4T1 cell viability after incubation with different concentrations of nanoparticles or AIEsomes in the dark or under light irradiation. (E) CLSM images of 4T1 cells under different conditions and stained with DCFDA. Reproduced with permission from ref. 149. Copyright 2018 Wiley-VCH.

morphological transitions, have been directly visualized based on an AIEgen-containing amphiphile.[153] This amphiphile was synthesized by incorporating TPE units into sodium dodecyl sulfonate (SDS). TPE–SDS showed negligible fluorescence emission in an aqueous solution at a very low concentration because it was effectively dispersed and the phenyl groups could freely rotate for energy relaxation. Upon increasing the TPE–SDS concentration, the fluorescence intensity gradually increased, where the amphiphiles began to aggregate and unimers of TPE–SDS were formed. When the concentration was above the CMC, the increasing rate of fluorescence decreased, and

 This journal is © The Royal Society of Chemistry 2020

Published on 23 January 2020. Downloaded by Yunnan University on 8/9/2025 11:18:24 PM.

the unimers assembled into micelles. This is because the TPE units present in the nonpolar interior of the micelles could more freely rotate than that in the unimers. CLSM images revealed that these micelles were spherically shaped with strong blue emission. Interestingly, the micellar transition was also directly observed by CLSM. Upon the continuous addition of salt into the TPE–SDS solution, the original spherical micelles were first fused into bigger rod-like micelles, which continued to grow into worm-like micelles. The results were also obtained by TEM and rheological measurements.

Hydrogels have been widely used in the fields of engineering materials to biotechnology and nanomedicine by virtue of their excellent hardness, strength, and toughness.[154] Until now, various methods such as crosslinking and complexation with other polymers have been developed to fabricate hydrogels. Despite the impressive progress in construction, the detailed gelation process is still unclear. Fluorescence techniques offer a direct insight into the gelation process. Very recently, our group[155] successfully monitored the gelation processes of CS LiOH–urea system based on AIEgens. The TPE–CS polymer was obtained by linking the TPE AIEgen moiety to the side chain of CS polymers. The labeling degrees of TPE–CS were elegantly designed, with the aim to minimize the TPE interference toward CS gelation, where CS and TPE–CS exhibited similar gelation behaviors. CLSM was used to visualize the gelation process in real time. It was found that the entire gelation process involved two stages: thermal gelation stage and rinse stage. TPE–CS solution initially showed a uniform light blue emission. At the thermal gelation stage, some areas appeared bright blue, which increased in size with the heating time. During the subsequent rinse stage, the removal of LiOH and urea further induced the contraction of blue areas and formation of a reticular structure, resulting in stable gel architecture. Optical transparency and elastic behaviors exhibited good consistence with fluorescence imaging. The embryonic structure and crystal were formed during the thermal gelation stage driven by the elevated temperature; the rinse stage increased these inter-/intramolecular hydrogen bonds, which resulted in increased toughness and volume shrinkage. This work provides a simple and straightforward method to investigate various gelation behaviors.

The properties of conjugated polymers are dependent on the building blocks of the elementary polymer chain, as well as their higher organizational structures in films or aggregates. Investigating the relationship between the properties of polymers and their organizational structures in the aggregated state is of great significance. Fluorescence emission provides a worthwhile opportunity to optimize the morphological transformation of polymer aggregates. Recently, a TPE-based polymer was developed to investigate the morphological transition in the self-assembly process from hollow nanospheres to nano-/microfibers (Fig. 23).[156] Initially, the polymer self-assembled

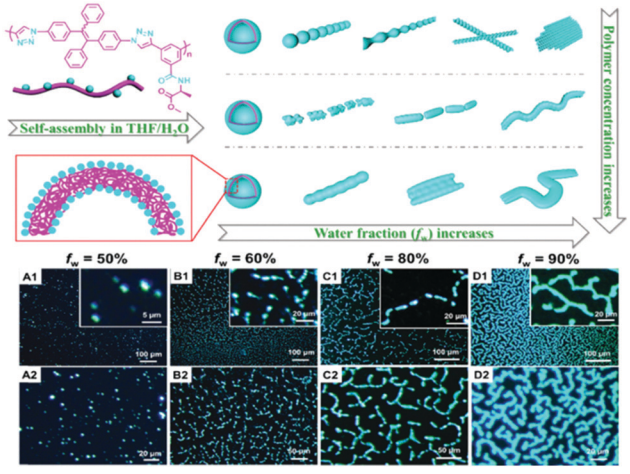

Fig. 23 Schematic representation and visualization of the self-assembly and morphological transition processes of TPE-containing polymers at different concentrations and water fractions. Reproduced with permission from ref. 156. Copyright 2018 Royal Society of Chemistry.

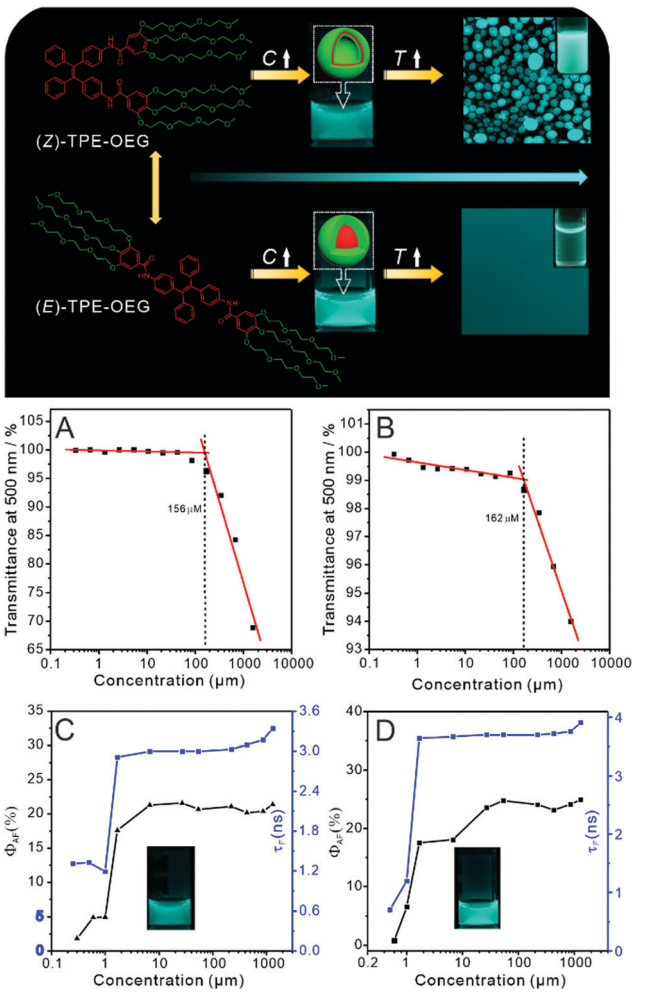

Fig. 24 Self-assembly and transformation of AIEgen-based micelles and vesicles. Concentration-dependent optical transmittance of (A) vesicles and (B) micelles in water. Fluorescence quantum yield and lifetime of (C) vesicles and (D) micelles in water for different polymer concentrations. Reproduced with permission from ref. 157. Copyright 2019 American Chemical Society.

Published on 23 January 2020. Downloaded by Yunnan University on 8/9/2025 11:18:24 PM.

into spherical structures with an average diameter of 180 nm. When the poor-solvent water content increased to 60%, the spherical nanoparticles fused with one another in a linear manner, forming "pearl-necklace"-like structures. While the water fraction was 80%, the pearl necklaces completely coalesced to form rods and helical nanowires. Finally, the helical nanofibers were further arranged in a side-by-side manner to form broom-like films at a water fraction of 90%. The morphological transformations were also observed at other polymer concentrations. Taking the polymer concentration of 5×10^{-4} M as an example, initially, the aggregates were hollow vesicles; with the addition of more water, they transformed into short nanofibers and long worm-like fibers. This work provides important insights into the rational design of ideal building blocks for the desired fluorescent architectures.

Most of the supramolecular materials, such as micelles, vesicles, fibers, and nanotubes, are constructed by the self-assembly of amphiphiles at a desired concentration. However, these amphiphiles are effectively dissolved in water and no aggregates are formed at lower concentrations. The distinctive properties of AIEgens allow them to facilitate the visualization of the formation of tiny aggregates and monitor the CAC concentration since the fluorescence of AIEgens is highly sensitive to intramolecular motion. It has been demonstrated that certain unimers can be formed before the formation of well-defined assemblies.[157] Two soluble TPE derivates, namely, (*Z*)-TPE–OEG and (*E*)-TPE–OEG, were synthesized by linking three OEG chains to the TPE segment. The CAC values of (*Z*)- and (*E*)-amphiphiles were determined to be 156 and 162 μM, respectively, by means of the transmittance method. However, the CAC value of both (*Z*)- and (*E*)-amphiphiles was determined to be 1.7 μM, which was extremely low as compared to that obtained using the transmittance method. TEM images showed that the corresponding morphologies of (*Z*)- and (*E*)-TPE–OEG exhibited homogeneous nanospheres with diameters of 3–6 nm at a concentration of 30 μM, which confirmed the existence of micelles below the CAC value measured by means of the transmittance method. This was because the amphiphiles were not molecularly dissolved in water even at lower concentrations (Fig. 24). Conversely, their molecules were packed together to form very tiny structures, which had a marginal impact on the transmittance measurement. It was confirmed that the formation

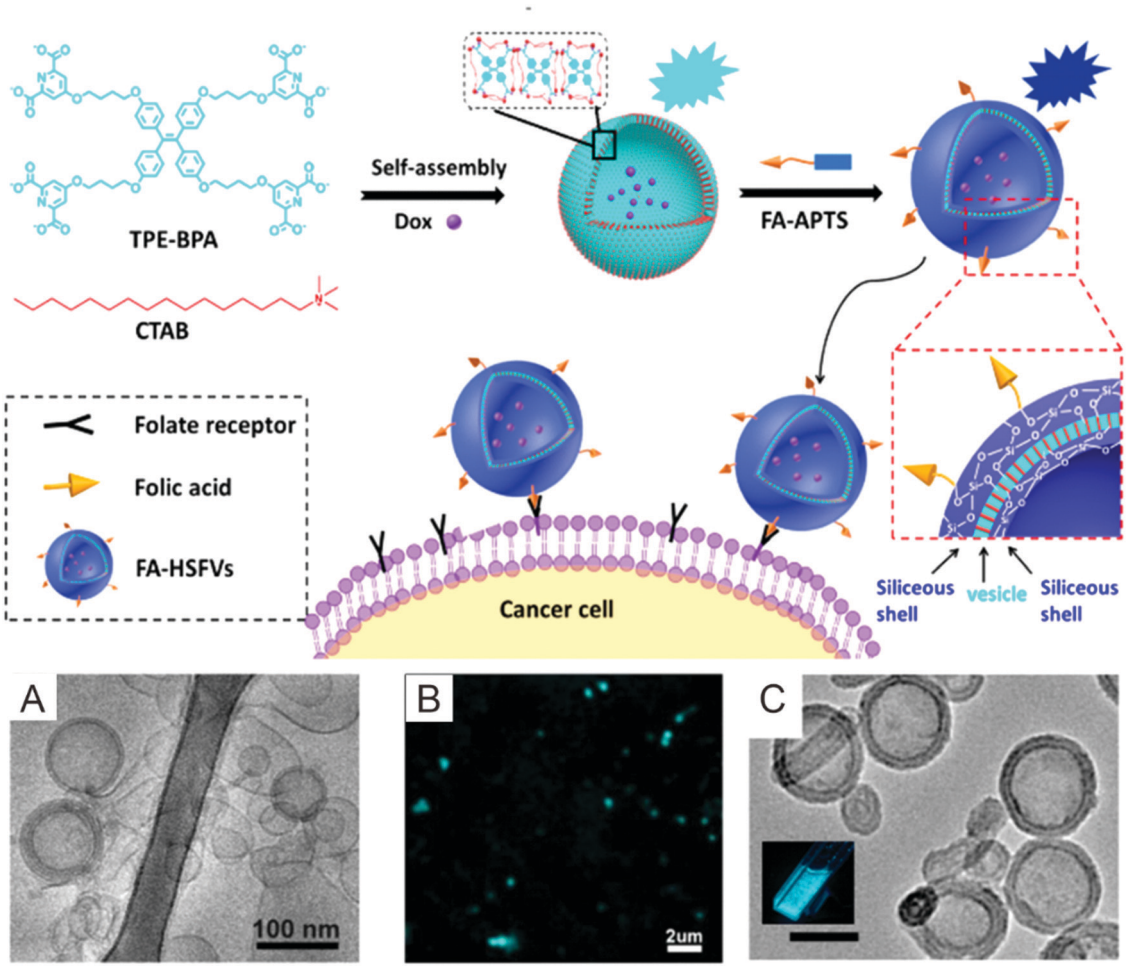

Fig. 25 Fluorescent vesicles as the template to prepare silicate fluorescent supramolecular vesicles and targeted combination with cancer cells. (A) Cryo-TEM images of the fluorescent vesicles. (B) CLSM image of the fluorescent vesicles. (C) TEM images of the silicate fluorescent supramolecular vesicles. Reproduced with permission from ref. 158. Copyright 2017 American Chemical Society.

 This journal is © The Royal Society of Chemistry 2020

Published on 23 January 2020. Downloaded by Yunnan University on 8/9/2025 11:18:24 PM.

of self-assembled nanostructures actually occurred at a concentration that was far lower than that detected by the conventional transmittance measurement. Moreover, the phase transitions were also visualized in these two systems. Therefore, AIEgen-based fluorescence is a highly sensitive method to investigate supramolecular assembly behaviors.

3.4. Platform for luminescent materials

AIEgen-based supramolecular fluorescent materials exhibit extremely high fluorescence efficiency, which enables them to be widely used as luminescent materials. Since these materials are fabricated through intermolecular interactions, numerous guest molecules can be feasibly introduced into such materials, allowing AIEgen-based supramolecular fluorescent materials to act as a platform to construct various luminescent materials such as inorganic nanoparticles and tunable emissive materials.

Inorganic materials have better mechanical properties than organic materials. However, inorganic materials are fairly difficult to fabricate with the desired structures and strong emission characteristics. Recently, Yan and coworkers[158] used fluorescent vesicles as the template to fabricate hollow-structured silica nanoparticles. As shown in Fig. 25, the fluorescent vesicles were self-assembled by AIEgens and oppositely charged surfactants in water, where the TPE segment was located on the inner side of the membrane. Due to the hydrophobicity of the inner membrane of the vesicles, the hydrophobic silicate compound TEOS entered the membrane and hydrolyzed to form a network polymer along the membrane. As a result, inorganic silica nanoparticles were formed, where the morphology of the vesicles was copied onto the nanoparticles. Simultaneously, the TPE was located in the silica layer of the nanoparticles, and their molecular motion was considerably restricted, enabling these nanoparticles to exhibit efficient emission characteristics. This strong fluorescence emission rendered the silica nanoparticles with excellent performance toward cellular imaging. Upon linking with the targeted agent, these silica nanoparticles were selectively enriched around the cancer cells, thereby releasing the loaded drugs for therapy.

Organic dyes could also be introduced into AIEgen-based supramolecular materials. A well-known example is an artificial light-harvesting system. An efficient artificial light-harvesting system was formulated on the basis of the noncovalent self-assembly of an oligo(phenylenevinylene) derivative (OPV-I), sulfato-β-CD (SCD), and Nile red (NiR) (Fig. 26A).[159] OPV-I exhibits excellent AIE properties at a high concentration, which can be further improved by SCD *via* aggregation-induced emission enhancement (AIEE) based on the SCD-induced OPV-I aggregation. The intense AIE effects enabled the OPV-I/SCD assembly to serve as a good donor. Meanwhile, NiR was loaded into the interior of the OPV-I/SCD assembly and it acted as a good acceptor, thereby establishing a FRET process with OPV-I/SCD nanoparticles to form a highly efficient artificial light-harvesting system. Given that only a small amount of NiR could be loaded onto the hydrophobic layer of the OPV-I/SCD assembly instead of being encapsulated in the cavity of SCD due to weak binding between the CD cavity and NiR, the donor/acceptor ratio of the light-harvesting system was very high (up to 125 : 1). This system also exhibited an energy transfer efficiency of 72% and an antenna effect of 32.5, which was similar to a natural light-harvesting system.

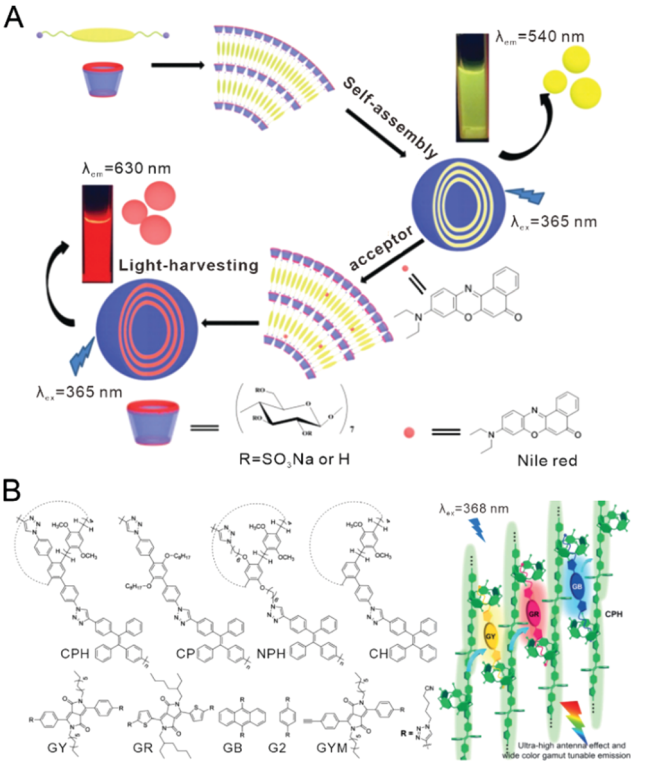

Fig. 26 AIEgen-based supramolecular materials as hosts to construct tunable emission systems. (A) AIEgen-based host–guest complexes as donors and NiR as an acceptor to fabricate light-harvesting nanoparticles. Reproduced with permission from ref. 159. Copyright 2017 Wiley-VCH. (B) TPE-based polymers as the host to combine three conjugated ditopic guests. Reproduced with permission from ref. 160. Copyright 2019 Wiley-VCH.

Very recently, a new strategy to build an efficient artificial light-harvesting system was demonstrated on the basis of a conjugated polymeric supramolecular network (CPSN) with the AIEE effect (Fig. 26B).[160] The supramolecular network was formed *via* the host–guest interaction between the conjugated ditopic guests (Gs) and a conjugated polymeric host (CPH) based on the pillar[5]arene and AEE moieties. The CPH could serve as an excellent donor due to its high ability of energy transfer reinforced by the molecular wire effect. CPH chains were further crosslinked or entangled *via* the efficient binding between Gs and the pillar[5]arene cavities. Gs acted as the acceptors and existed only in trace amounts within the CPSN, thereby yielding a high donor/acceptor ratio of 10 000 : 1. The CPSN also exhibited an unprecedented antenna effect (35.9 in solution and 90.4 in solid film). Moreover, the emission color of CPSN could be further tuned by altering the various Gs or adjusting the donor/acceptor ratio. In particular, the absorption spectra of the guest GR with red emission and guest GY with yellow emission effectively overlapped with the emission spectrum of CPH, thereby establishing efficient energy transfer from the CPH to GY and GR. Nevertheless, the emission

Published on 23 January 2020. Downloaded by Yunnan University on 8/9/2025 11:18:24 PM.

spectrum of guest GB with blue emission hardly matched the absorption spectrum of CPH. By adjusting the ratio of various Gs and the CPH repeating units (RU), accurately tunable emission colors and a wide color gamut of CPSN could be achieved. In particular, when CPSN was constructed with 2.5 μM GB, 50 nM GR, and 10 μM RU, an accurate white emission of (0.33, 0.33) in the CIE coordinates could be obtained. The color gamut was wide and achieved approximately 96% sRGB area.

4. Conclusions and perspectives

AIEgens are an emerging class of luminescent materials that are nonemissive in solutions but intensely emit upon aggregate formation. The AIE effect has significantly stimulated the development of supramolecular luminescent materials, benefiting from their intrinsic advantages such as bright emission in the aggregate form, high photobleaching threshold, and high signal-to-noise ratio. In principle, the configurations of AIEgens are highly twisted or propeller-shaped in space. The nonplanar configuration avoids fluorescence quenching in the aggregate stage, yielding AIEgens-based supramolecular materials with high luminescence efficiency. Simultaneously, the nonplanar configuration also prevents AIEgens from packing together, considerably deterring the construction of highly ordered supramolecular architectures. Ensuring that AIEgens can have sufficient aggregation ability can overcome these obstacles: for example, AIEgens can be decorated with moieties that possess a strong tendency toward aggregation or AIEgens can be incorporated into the fabricated supramolecular structures. These strategies have prompted the emergence of a large number of AIEgens-based supramolecular luminescent materials with diverse architectures at all scales, including macrocycle, self-assembled, and macromolecular systems. The excellent fluorescence in the aggregated state usually renders AIEgen-based supramolecular materials to act as ideal candidates for bioimaging, as well as powerful instruments to directly visualize the assembly process of supramolecular materials. In addition, AIEgens possess the advantages of tunable emission and photodynamic and photothermal therapies. Combined with dynamic and reversible capacity, AIEgen-based supramolecular materials can create newer applications in a large range of fields such as sensors, theranostics, and luminescent materials.

Despite the fact that remarkable progress has already been made, several aspects have been deemed to be essential for fabricating advanced AIEgens-based supramolecular luminescent materials. The examples covered in this review mainly involve short-wavelength AIEgens, such as TPE and its derivates, which restrict *in vivo* applications. Developing supramolecular luminescent materials based on red or FR/NIR-emissive AIEgens is highly desirable because their deep penetration and low autofluorescence can considerably widen the scope of preclinical research and clinical applications. In addition to highly fluorescent emissions, AIEgens possess the amazing capacity of photodynamic, photoacoustic, and photothermal therapeutic efficiencies, which can accelerate the development of advanced theranostic platforms with an extremely simple and innovative strategy. With the aim to gain a better understanding of supramolecular chemistry, it is particularly important to directly visualize the self-assembly processes of AIEgens-based supramolecular materials. In addition, manipulating and controlling the size distribution and morphologies of AIEgens-based supramolecular materials has become imperative. Moreover, increased attention should be focused on the development of stimuli-responsive AIEgens-based supramolecular materials to improve their performances in the field of sensors, theranostics, and bioimaging. We hope that this review can trigger more interest and garner more ideas from researchers and further advance the development of supramolecular chemistry.

Conflicts of interest

There are no conflicts to declare.

Acknowledgements

This work was financially supported by National Natural Science Foundation of China (Grant No. 21801169, 21902106), Natural Science Foundation of Shenzhen University (Grant No. 2019004), and China Postdoctoral Science Foundation (No. 2019M653005).

References

1 D. A. Uhlenheuer, K. Petkau and L. Brunsveld, *Chem. Soc. Rev.*, 2010, **39**, 2817–2826.
2 H. Wu and M. Fuxreiter, *Cell*, 2016, **165**, 1055–1066.
3 J. Boekhoven, W. E. Hendriksen, G. J. M. Koper, R. Eelkema and J. H. V. Esch, *Science*, 2015, **349**, 1075–1079.
4 J. M. A. Carnall, C. A. Waudby, A. M. Belenguer, M. C. A. Stuart, J. R. M. J.-P. Peyralans and S. Otto, *Science*, 2010, **327**, 1502–1506.
5 D. B. Amabilino, D. K. Smith and J. W. Steed, *Chem. Soc. Rev.*, 2017, **46**, 2404–2420.
6 L. You, D. J. Zha and E. V. Anslyn, *Chem. Rev.*, 2015, **115**, 7840–7892.
7 J.-M. Lehn, *Science*, 2002, **295**, 2400–2403.
8 M. H. Liu, L. Zhang and T. Y. Wang, *Chem. Rev.*, 2015, **115**, 7304–7397.
9 L. Brunsveld, B. J. B. Folmer, E. W. Meijer and R. P. Sijbesma, *Chem. Rev.*, 2001, **101**, 4071–4097.
10 W. Zhang and T. Aida, *Science*, 2012, **337**, 1462–1463.
11 J. Zhou, G. C. Yu and F. H. Huang, *Chem. Soc. Rev.*, 2017, **46**, 7021–7053.
12 R. M. da Silva, D. van der Zwaag, L. Albertazzi, S. S. Lee, E. W. Meijer and S. I. Stupp, *Nat. Commun.*, 2016, **7**, 11561.
13 T. Ogoshi, T. A. Yamagishi and Y. Nakamoto, *Chem. Rev.*, 2016, **116**, 7937–8002.
14 J. W. Chen, F. K.-C. Leung, M. C. A. Stuart, T. Kajitani, T. Fukushima, E. van der Giessen and B. L. Feringa, *Nat. Chem.*, 2017, **10**, 132–138.

 This journal is © The Royal Society of Chemistry 2020

Published on 23 January 2020. Downloaded by Yunnan University on 8/9/2025 11:18:24 PM.

15 S. Datta, M. L. Saha and P. J. Stang, *Acc. Chem. Res.*, 2018, **51**, 2047–2063.
16 R. Freeman, M. Han, Z. Álvarez, J. A. Lewis, J. R. Wester, N. Stephanopoulos, M. T. McClendon, C. Lynsky, J. M. Godbe, H. Sangji, E. Luijten and S. I. Stupp, *Science*, 2018, **362**, 808–813.
17 H. Cabral, N. Nishiyama and K. Kataoka, *Acc. Chem. Res.*, 2011, **44**, 999–1008.
18 C. J. C. Edwards-Gayle and I. W. Hamley, *Org. Biomol. Chem.*, 2017, **15**, 5867–5876.
19 M. J. Webber and R. Langer, *Chem. Soc. Rev.*, 2017, **46**, 6600–6620.
20 X. Ma and H. Tian, *Acc. Chem. Res.*, 2014, **47**, 1971–1981.
21 J. S. Wu, B. Kwon, W. M. Liu, E. V. Anslyn, P. F. Wang and J. S. Kim, *Chem. Rev.*, 2015, **115**, 7893–7943.
22 K. L. Diehl and E. V. Anslyn, *Chem. Soc. Rev.*, 2013, **42**, 8596–8611.
23 I. V. Kolesnichenko and E. V. Anslyn, *Chem. Soc. Rev.*, 2017, **46**, 2385–2390.
24 L. A. Joyce, S. H. Shabbir and E. V. Anslyn, *Chem. Soc. Rev.*, 2010, **39**, 3621–3632.
25 A. C. Coleman, J. M. Beierle, M. C. A. Stuart, B. Maciá, G. Caroli, J. T. Mika, D. J. van Dijken, J. Chen, W. R. Browne and B. L. Feringa, *Nat. Nanotechnol.*, 2011, **6**, 547–552.
26 S. I. Stupp and L. C. Palmer, *Chem. Mater.*, 2013, **26**, 507–518.
27 L. Albertazzi, D. V. D. Zwaag, C. M. A. Leenders, R. Fitzner, R. W. V. D. Hofstad and E. W. Meijer, *Science*, 2014, **344**, 491–495.
28 F. S. Kim, G. Ren and S. A. Jenekhe, *Chem. Mater.*, 2011, **23**, 682–732.
29 M. A. Kobaisi, S. V. Bhosale, K. Latham, A. M. Raynor and S. V. Bhosale, *Chem. Rev.*, 2016, **116**, 11685–11796.
30 F. J. M. Hoeben, P. Jonkheijm, E. W. Meijer and A. P. H. J. Schenning, *Chem. Rev.*, 2005, **105**, 1491–1546.
31 D. González-Rodríguez and A. P. H. J. Schenning, *Chem. Mater.*, 2011, **23**, 310–325.
32 R. T. K. Kwok, C. W. T. Leung, J. W. Y. Lam and B. Z. Tang, *Chem. Soc. Rev.*, 2015, **44**, 4228–4238.
33 J. D. Luo, Z. L. Xie, J. W. Y. Lam, L. Cheng, H. Y. Chen, C. F. Qiu, H. S. Kwok, X. W. Zhan, Y. Q. Liu, D. B. Zhu and B. Z. Tang, *Chem. Commun.*, 2001, 1740–1741.
34 Y. Hong, J. W. Y. Lam and B. Z. Tang, *Chem. Soc. Rev.*, 2011, **40**, 5361–5388.
35 J. Mei, Y. N. Hong, J. W. Y. Lam, A. J. Qin, Y. H. Tang and B. Z. Tang, *Adv. Mater.*, 2014, **26**, 5429–5479.
36 J. Mei, N. L. Leung, R. T. Kwok, J. W. Y. Lam and B. Z. Tang, *Chem. Rev.*, 2015, **115**, 11718–11940.
37 B. Z. Tang, X. Zhan, G. Yu, P. P. Sze Lee, Y. Liu and D. Zhu, *J. Mater. Chem.*, 2001, **11**, 2974–2978.
38 B.-K. An, S.-K. Kwon, S.-D. Jung and S. Y. Park, *J. Am. Chem. Soc.*, 2002, **124**, 14110–14415.
39 J. Liang, B. Z. Tang and B. Liu, *Chem. Soc. Rev.*, 2015, **44**, 2798–2811.
40 D. Wang and B. Z. Tang, *Acc. Chem. Res.*, 2019, **52**, 2559–2570.
41 D. Ding, K. Li, B. Liu and B. Z. Tang, *Acc. Chem. Res.*, 2013, **46**, 2441–2453.
42 S. J. Liu, X. Zhou, H. K. Zhang, H. L. Ou, J. W. Y. Lam, Y. Liu, L. Q. Shi, D. Ding and B. Z. Tang, *J. Am. Chem. Soc.*, 2019, **141**, 5359–5368.
43 D. Wang, M. M. S. Lee, W. Xu, G. G. Shan, X. Y. Zheng, R. T. K. Kwok, J. W. Y. Lam, X. L. Hu and B. Z. Tang, *Angew. Chem., Int. Ed.*, 2019, **58**, 5628–5632.
44 Z. Zhao, C. Chen, W. T. Wu, F. F. Wang, L. L. Du, X. Y. Zhang, Y. Xiong, X. W. He, Y. J. Cai, R. T. K. Kwok, J. W. Y. Lam, X. K. Gao, P. C. Sun, D. L. Phillips, D. Ding and B. Z. Tang, *Nat. Commun.*, 2019, **10**, 768.
45 X. W. He, L. H. Xiong, Z. Zhao, Z. Y. Wang, L. Luo, J. W. Y. Lam, R. T. K. Kwok and B. Z. Tang, *Theranostics*, 2019, **9**, 3223–3248.
46 D. Wang, M. M. S. Lee, G. G. Shan, R. T. K. Kwok, J. W. Y. Lam, H. F. Su, Y. C. Cai and B. Z. Tang, *Adv. Mater.*, 2018, **30**, 1802105.
47 T. F. Zhang, Y. Y. Li, Z. Zheng, R. Q. Ye, Y. R. Zhang, R. T. K. Kwok, J. W. Y. Lam and B. Z. Tang, *J. Am. Chem. Soc.*, 2019, **141**, 5612–5616.
48 S. J. Liu, H. K. Zhang, Y. Y. Li, J. K. Liu, L. L. Du, M. Chen, R. T. K. Kwok, J. W. Y. Lam, D. L. Phillips and B. Z. Tang, *Angew. Chem., Int. Ed.*, 2018, **57**, 15189–15193.
49 S. Srivastava, A. Santos, K. Critchley, K.-S. Kim, P. Podsiadlo, K. Sun, J. Lee, C. L. Xu, G. D. Lilly, S. C. Glotzer and N. A. Kotov, *Science*, 2010, **327**, 1355–1359.
50 Y. X. Zong, Y. Y. Zhou, M. G. Ju, H. F. Garces, A. R. Krause, F. X. Ji, G. L. Cui, X. C. Zeng, N. P. Padture and S. P. Pang, *Angew. Chem., Int. Ed.*, 2016, **55**, 14723–14727.
51 H. B. Qiu, Z. M. Hudson, M. A. Winnik and I. Manners, *Science*, 2015, **347**, 1329–1332.
52 D. Y. Yan, Y. F. Zhou and J. Hou, *Science*, 2004, **303**, 65–67.
53 K. T. Li, Y. J. Lin and C. Lu, *Chem. – Asian J.*, 2019, **14**, 715–729.
54 S. J. Liu, Y. Y. Li, H. K. Zhang, Z. Zhao, X. F. Lu, J. W. Y. Lam and B. Z. Tang, *ACS Mater. Lett.*, 2019, **1**, 425–431.
55 N. L. C. Leung, N. Xie, W. Z. Yuan, Y. Liu, Q. Y. Wu, Q. Peng, Q. Miao, J. W. Y. Lam and B. Z. Tang, *Chem. – Eur. J.*, 2014, **20**, 15349–15353.
56 Anuradha, D. D. La, M. A. Kobaisi, A. Gupta and S. V. Bhosale, *Chem. – Eur. J.*, 2017, **23**, 3950–3956.
57 X. Y. Lou and Y. W. Yang, *Adv. Opt. Mater.*, 2018, **6**, 1800668.
58 Y. J. Zhou, K. C. Jie, R. Zhao and F. H. Huang, *Adv. Mater.*, 2019, 1904824.
59 K. C. Jie, Y. J. Zhou, Y. Yao and F. H. Huang, *Chem. Soc. Rev.*, 2015, **44**, 3568–3587.
60 G. S. Chen and M. Jiang, *Chem. Soc. Rev.*, 2011, **40**, 2254–2266.
61 G. C. Yu, K. C. Jie and F. H. Huang, *Chem. Rev.*, 2015, **115**, 7240–7303.
62 H. T. Feng, Y. X. Yuan, J. B. Xiong, Y. S. Zheng and B. Z. Tang, *Chem. Soc. Rev.*, 2018, **47**, 7452–7476.
63 G. D. Liang, J. W. Y. Lam, W. Qin, J. Li, N. Xie and B. Z. Tang, *Chem. Commun.*, 2014, **50**, 1725–1727.
64 Y. Yu, Y. W. Li, X. Q. Wang, H. Nian, L. Wang, J. Li, Y. X. Zhao, X. R. Yang, S. M. Liu and L. P. Cao, *J. Org. Chem.*, 2017, **82**, 5590–5596.

Published on 23 January 2020. Downloaded by Yunnan University on 8/9/2025 11:18:24 PM.

65 H. T. Feng, S. Song, Y. C. Chen, C. H. Shen and Y. S. Zheng, *J. Mater. Chem. C*, 2014, **2**, 2353–2359.
66 H. T. Feng, X. Y. Zheng, X. G. Gu, M. Chen, J. W. Y. Lam, X. H. Huang and B. Z. Tang, *Chem. Mater.*, 2018, **30**, 1285–1290.
67 X. J. Shi, X. D. Zhang, X. L. Ni, H. K. Zhang, P. F. Wei, J. K. Liu, H. Xing, H. Q. Peng, J. W. Y. Lam, P. F. Zhang, Z. Y. Wang, H. X. Hao and B. Z. Tang, *Macromolecules*, 2019, **52**, 8814–8825.
68 B. P. Jiang, D. S. Guo, Y. C. Liu, K. P. Wang and Y. Liu, *ACS Nano*, 2014, **8**, 1609–1618.
69 Y. W. Li, Y. H. Dong, X. R. Miao, Y. L. Ren, B. L. Zhang, P. P. Wang, Y. Yu, B. Li, L. Isaacs and L. P. Cao, *Angew. Chem., Int. Ed.*, 2018, **57**, 729–733.
70 L. Shao, J. F. Sun, B. Hua and F. H. Huang, *Chem. Commun.*, 2018, **54**, 4866–4869.
71 N. Song, D. X. Chen, Y. C. Qiu, X. Y. Yang, B. Xu, W. Tian and Y. W. Yang, *Chem. Commun.*, 2014, **50**, 8231–8234.
72 M. C.-L. Yeung and V. W.-W. Yam, *Chem. Soc. Rev.*, 2015, **44**, 4192–4202.
73 W. Bai, Z. Y. Wang, J. Q. Tong, J. Mei, A. J. Qin, J. Z. Sun and B. Z. Tang, *Chem. Commun.*, 2015, **51**, 1089–1091.
74 L. N. Xu, D. Chen, Q. Zhang, T. He, C. J. Lu, X. Shen, D. T. Tang, H. Y. Qiu, M. M. Zhang and S. C. Yin, *Polym. Chem.*, 2018, **9**, 399–403.
75 H. M. Wang, Z. Q. Q. Feng and B. Xu, *Chem. Soc. Rev.*, 2017, **46**, 2421–2436.
76 S. Fleming and R. V. Ulijn, *Chem. Soc. Rev.*, 2014, **43**, 8150–8177.
77 Y. Sun, C. Y. Chen and P. J. Stang, *Acc. Chem. Res.*, 2019, **52**, 802–817.
78 L. L. Yang, X. X. Tan, Z. Q. Wang and X. Zhang, *Chem. Rev.*, 2015, **115**, 7196–7239.
79 Y. Yan, J. B. Huang and B. Z. Tang, *Chem. Commun.*, 2016, **52**, 11870–11884.
80 T. Shimizu, N. Kameta, W. Ding and M. Masuda, *Langmuir*, 2016, **32**, 12242–12264.
81 S. Cantekin, T. F. A. de Greef and A. R. A. Palmans, *Chem. Soc. Rev.*, 2012, **41**, 6125–6137.
82 V. Percec, D. A. Wilson, P. Leowanawat, C. J. Wilson, A. D. Hughes, M. S. Kaucher, D. A. Hammer, D. H. Levine, A. J. Kim, F. S. Bates, K. P. Davis, T. P. Lodge, M. L. Klein, R. H. DeVane, E. Aqad, B. M. Rosen, A. O. Argintaru, M. J. Sienkowska, K. Rissanen, S. Nummelin and J. Ropponen, *Science*, 2010, **328**, 1009–1014.
83 A. Seoane, R. J. Brea, A. Fuertes, K. A. Podolsky and N. K. Devaraj, *J. Am. Chem. Soc.*, 2018, **140**, 8388–8391.
84 R. J. Brea, A. Bhattacharya, R. Bhattacharya, J. J. Song, S. K. Sinha and N. K. Devaraj, *J. Am. Chem. Soc.*, 2018, **140**, 17356–17360.
85 J. Li, K. Liu, Y. C. Han, B. Z. Tang, J. B. Huang and Y. Yan, *ACS Appl. Mater. Interfaces*, 2016, **8**, 27987–27995.
86 M. Zhang, X. P. Yin, T. Tian, Y. Liang, W. N. Li, Y. Lan, J. Li, M. M. Zhou, Y. Ju and G. T. Li, *Chem. Commun.*, 2015, **51**, 10210–10213.
87 Y. W. Li, Y. H. Dong, L. Cheng, C. Y. Qin, H. Nian, H. Y. Zhang, Y. Yu and L. P. Cao, *J. Am. Chem. Soc.*, 2019, **141**, 8412–8415.
88 H. K. Li, B. S. Li and B. Z. Tang, *Chem. – Asian J.*, 2019, **14**, 674–688.
89 L. Zhang, L. Qin, X. F. Wang, H. Cao and M. H. Liu, *Adv. Mater.*, 2014, **26**, 6959–6964.
90 X. B. Shang, I. H. Song, H. Ohtsu, Y. H. Lee, T. M. Zhao, T. Kojima, J. H. Jung, M. Kawano and J. H. Oh, *Adv. Mater.*, 2017, **29**, 1605828.
91 H. K. Li, S. Xue, H. M. Su, B. Shen, Z. H. Cheng, J. W. Y. Lam, K. S. Wong, H. K. Wu, B. S. Li and B. Z. Tang, *Small*, 2016, **12**, 6593–6601.
92 H. K. Li, J. Cheng, H. Q. Deng, E. G. Zhao, B. Shen, J. W. Y. Lam, K. S. Wong, H. K. Wu, B. S. Li and B. Z. Tang, *J. Mater. Chem. C*, 2015, **3**, 2399–2404.
93 J. Zhang, Q. M. Liu, W. J. Wu, J. H. Peng, H. K. Zhang, F. Y. Song, B. Z. He, X. Y. Wang, H. H. Y. Sung, M. Chen, B. S. Li, S. H. Liu, J. W. Y. Lam and B. Z. Tang, *ACS Nano*, 2019, **13**, 3618–3628.
94 S. Yagai, M. Yamauchi, A. Kobayashi, T. Karatsu, A. Kitamura, T. Ohba and Y. Kikkawa, *J. Am. Chem. Soc.*, 2012, **134**, 18205–18208.
95 M. Baroncini, S. d'Agostino, G. Bergamini, P. Ceroni, A. Comotti, P. Sozzani, I. Bassanetti, F. Grepioni, T. M. Hernandez, S. Silvi, M. Venturi and A. Credi, *Nat. Chem.*, 2015, **7**, 634–640.
96 N. Bäumer, K. K. Kartha, N. K. Allampally, S. Yagai, R. Q. Albuquerque and G. Fernández, *Angew. Chem., Int. Ed.*, 2019, **58**, 15626–15630.
97 H. Q. Peng, X. Y. Zheng, T. Han, R. T. K. Kwok, J. W. Y. Lam, X. H. Huang and B. Z. Tang, *J. Am. Chem. Soc.*, 2017, **139**, 10150–10156.
98 J. L. Han, J. You, X. G. Li, P. F. Duan and M. H. Liu, *Adv. Mater.*, 2017, **29**, 1606503.
99 M. Q. Xie, Y. X. Che, K. Liu, L. X. Jiang, L. M. Xu, R. R. Xue, M. Drechsler, J. B. Huang, B. Z. Tang and Y. Yan, *Adv. Funct. Mater.*, 2018, **28**, 1803370.
100 S. L. Li, T. X. Xiao, C. Lin and L. Wang, *Chem. Soc. Rev.*, 2012, **41**, 5950–5968.
101 P. Makam and E. Gazit, *Chem. Soc. Rev.*, 2018, **47**, 3406–3420.
102 B. N. S. Thota, L. H. Urner and R. Haag, *Chem. Rev.*, 2015, **116**, 2079–2102.
103 S. P. W. Wijnands, E. W. Meijer and M. Merkx, *Bioconjugate Chem.*, 2019, **30**, 1905–1914.
104 M. P. Hendricks, K. Sato, L. C. Palmer and S. I. Stupp, *Acc. Chem. Res.*, 2017, **50**, 2440–2448.
105 C. H. Cai, J. P. Lin, Y. Q. Lu, Q. Zhang and L. Q. Wang, *Chem. Soc. Rev.*, 2016, **45**, 5985–6012.
106 X. W. Du, J. Zhou, J. F. Shi and B. Xu, *Chem. Rev.*, 2015, **115**, 13165–13307.
107 V. Mikhalevich, I. Craciun, M. Kyropoulou, C. G. Palivan and W. Meier, *Biomacromolecules*, 2017, **18**, 3471–3480.
108 C. Q. Zhang, C. Liu, X. D. Xue, X. Zhang, S. D. Huo, Y. G. Jiang, W. Q. Chen, G. Z. Zou and X. J. Liang, *ACS Appl. Mater. Interfaces*, 2013, **6**, 757–762.
109 H. Sai, K. W. Tan, K. Hur, E. Asenath-Smith, R. Hovden, Y. Jiang, M. Riccio, D. A. Muller, V. Elser, L. A. Estroff, S. M. Gruner and U. Wiesner, *Science*, 2013, **341**, 530–534.

 This journal is © The Royal Society of Chemistry 2020

Published on 23 January 2020. Downloaded by Yunnan University on 8/9/2025 11:18:24 PM.

110 J. G. Kennemur, *Macromolecules*, 2019, **52**, 1354–1370.
111 X. F. Ji, B. B. Shi, H. Wang, D. Y. Xia, K. C. Jie, Z. L. Wu and F. H. Huang, *Adv. Mater.*, 2015, **27**, 8062–8066.
112 X. F. Ji, Z. Li, X. L. Liu, H. Q. Peng, F. Y. Song, J. Qi, J. W. Y. Lam, L. L. Long, J. L. Sessler and B. Z. Tang, *Adv. Mater.*, 2019, **31**, 1902365.
113 Y. M. Zhao, W. Zhu, L. X. Ren and K. Zhang, *Polym. Chem.*, 2016, **7**, 5386–5395.
114 Y. G. He, S. Y. Shi, N. Liu, Y. S. Ding, J. Yin and Z. Q. Wu, *Macromolecules*, 2015, **49**, 48–58.
115 N. Zhang, H. Chen, Y. J. Fan, L. Zhou, S. Trepout, J. Guo and M. H. Li, *ACS Nano*, 2018, **12**, 4025–4035.
116 M. Huo, Q. Q. Ye, H. L. Che, X. S. Wang, Y. Wei and J. Y. Yuan, *Macromolecules*, 2017, **50**, 1126–1133.
117 L. M. Xu, L. X. Jiang, M. Drechsler, Y. Sun, Z. R. Liu, J. B. Huang, B. Z. Tang, Z. B. Li, M. A. Cohen Stuart and Y. Yan, *J. Am. Chem. Soc.*, 2014, **136**, 1942–1947.
118 L. J. Chen, Y. Y. Ren, N. W. Wu, B. Sun, J. Q. Ma, L. Zhang, H. Tan, M. Liu, X. Li and H. B. Yang, *J. Am. Chem. Soc.*, 2015, **137**, 11725–11735.
119 N. Goswami, Q. F. Yao, Z. T. Luo, J. G. Li, T. K. Chen and J. P. Xie, *J. Phys. Chem. Lett.*, 2016, **7**, 962–975.
120 W. H. Xu, M. M. S. Lee, Z. H. Zhang, H. H. Y. Sung, I. D. Williams, R. T. K. Kwok, J. W. Y. Lam, D. Wang and B. Z. Tang, *Chem. Sci.*, 2019, **10**, 3494–3501.
121 M. Gao and B. Z. Tang, *ACS Sens.*, 2017, **2**, 1382–1399.
122 C. L. Zhu, R. T. K. Kwok, J. W. Y. Lam and B. Z. Tang, *ACS Appl. Bio Mater.*, 2018, **1**, 1768–1786.
123 H. Lee, B. In, P. K. Mehta, M. Y. L. N. Kishore and K.-H. Lee, *ACS Appl. Mater. Interfaces*, 2018, **10**, 2282–2290.
124 A. T. Han, H. M. Wang, R. T. K. Kwok, S. L. Ji, J. Li, D. L. Kong, B. Z. Tang, B. Liu, Z. M. Yang and D. Ding, *Anal. Chem.*, 2016, **88**, 3872–3878.
125 J. Shi, Q. C. Deng, Y. Li, Z. F. Chai, C. Y. Wan, H. J. Shangguan, L. Li and B. Tang, *Chem. – Asian J.*, 2018, **14**, 847–852.
126 J. D. Zhang, J. Mei, X. L. Hu, X. P. He and H. Tian, *Small*, 2016, **12**, 6562–6567.
127 B. P. Jiang, X. Y. Tan, X. C. Shen, W. Q. Lei, W. Q. Liang, S. C. Ji and H. Liang, *ACS Macro Lett.*, 2016, **5**, 450–454.
128 S. H. Jung, K. Y. Kwon and J. H. Jung, *Chem. Commun.*, 2015, **51**, 952–955.
129 X. Li, Z. Li and Y. W. Yang, *Adv. Mater.*, 2018, **30**, 1800177.
130 D. H. Dai, Z. Li, J. Yang, C. Y. Wang, J. R. Wu, Y. Wang, D. M. Zhang and Y. W. Yang, *J. Am. Chem. Soc.*, 2019, **141**, 4756–4763.
131 C. Q. Zhang, T. B. Zhang, S. B. Jin, X. D. Xue, X. L. Yang, N. Q. Gong, J. C. Zhang, P. C. Wang, J. H. Tian, J. F. Xing and X. J. Liang, *ACS Appl. Mater. Interfaces*, 2017, **9**, 4425–4432.
132 T. B. Zhang, W. S. Guo, C. Q. Zhang, J. Yu, J. Xu, S. Y. Li, J. H. Tian, P. C. Wang, J. F. Xing and X. J. Liang, *ACS Appl. Mater. Interfaces*, 2017, **9**, 16006–16014.
133 X. Wang, Y. Y. Yang, Y. P. Zhuang, P. Y. Gao, F. Yang, H. Shen, H. X. Guo and D. C. Wu, *Biomacromolecules*, 2016, **17**, 2920–2929.
134 Kenry, Y. K. Duan and B. Liu, *Adv. Mater.*, 2018, **30**, 1802394.
135 Z. Zhao, S. M. Gao, X. Y. Zheng, P. F. Zhang, W. T. Wu, R. T. K. Kwok, Y. Xiong, N. L. C. Leung, Y. C. Chen, X. K. Gao, J. W. Y. Lam and B. Z. Tang, *Adv. Funct. Mater.*, 2018, **28**, 1705609.
136 W. W. H. Lee, Z. Zhao, Y. J. Cai, Z. Xu, Y. Yu, Y. Xiong, R. T. K. Kwok, Y. Chen, N. L. C. Leung, D. G. Ma, J. W. Y. Lam, A. J. Qin and B. Z. Tang, *Chem. Sci.*, 2018, **9**, 6118–6125.
137 H. G. Lu, Y. D. Zheng, X. W. Zhao, L. J. Wang, S. Q. Ma, X. Q. Han, B. Xu, W. J. Tian and H. Gao, *Angew. Chem., Int. Ed.*, 2016, **55**, 155–159.
138 J. Qi, Y. Fang, R. T. K. Kwok, X. Y. Zhang, X. L. Hu, J. W. Y. Lam, D. Ding and B. Z. Tang, *ACS Nano*, 2017, **11**, 7177–7188.
139 J. Qi, C. W. Sun, A. Zebibula, H. Q. Zhang, R. T. K. Kwok, X. Y. Zhao, W. Xi, J. W. Y. Lam, J. Qian and B. Z. Tang, *Adv. Mater.*, 2018, **30**, 1706856.
140 Y. Guan, H. G. Lu, W. Li, Y. D. Zheng, Z. Jiang, J. L. Zou and H. Gao, *ACS Appl. Mater. Interfaces*, 2017, **9**, 26731–26739.
141 G. L. Niu, R. Y. Zhang, J. P. C. Kwong, J. W. Y. Lam, C. P. Chen, J. G. Wang, Y. C. Chen, X. Feng, R. T. K. Kwok, H. H. Y. Sung, I. D. Williams, M. R. J. Elsegood, J. N. Qu, C. Ma, K. S. Wong, X. Q. Yu and B. Z. Tang, *Chem. Mater.*, 2018, **30**, 4778–4787.
142 Y. B. Hu, T. Han, N. Yan, J. K. Liu, X. L. Liu, W. X. Wang, J. W. Y. Lam and B. Z. Tang, *Adv. Funct. Mater.*, 2019, **29**, 1902240.
143 J. Qi, C. W. Sun, D. Y. Li, H. Q. Zhang, W. B. Yu, A. Zebibula, J. W. Y. Lam, W. Xi, L. Zhu, F. H. Cai, P. F. Wei, C. L. Zhu, R. T. K. Kwok, L. L. Streich, R. Prevedel, J. Qian and B. Z. Tang, *ACS Nano*, 2018, **12**, 7936–7945.
144 T. Yu, W. H. Zhuang, X. Su, B. X. Ma, J. Hu, H. Y. He, G. C. Li and Y. B. Wang, *Bioconjugate Chem.*, 2019, **30**, 2075–2087.
145 X. D. Chi, H. C. Zhang, G. I. Vargas-Zúñiga, G. M. Peters and J. L. Sessler, *J. Am. Chem. Soc.*, 2016, **138**, 5829–5832.
146 F. Hu, S. D. Xu and B. Liu, *Adv. Mater.*, 2018, **30**, 1801350.
147 Z. Y. Liu, H. Zou, Z. Zhao, P. F. Zhang, G. G. Shan, R. T. K. Kwok, J. W. Y. Lam, L. Zheng and B. Z. Tang, *ACS Nano*, 2019, **13**, 11283–11293.
148 Y. Yuan, C.-J. Zhang and B. Liu, *Angew. Chem., Int. Ed.*, 2015, **54**, 11419–11423.
149 X. L. Cai, D. Mao, C. Wang, D. L. Kong, X. M. Cheng and B. Liu, *Angew. Chem., Int. Ed.*, 2018, **57**, 16396–16400.
150 B. J. Palmer and J. Liu, *Langmuir*, 1996, **12**, 746–753.
151 K. Sakai, K. Nomura, R. G. Shrestha, T. Endo, K. Sakamoto, H. Sakai and M. Abe, *Langmuir*, 2012, **28**, 17617–17622.
152 Y. Qiao, Y. Y. Lin, Y. J. Wang, Z. B. Li and J. B. Huang, *Langmuir*, 2011, **27**, 1718–1723.
153 W. J. Guan, W. J. Zhou, C. Lu and B. Z. Tang, *Angew. Chem., Int. Ed.*, 2015, **54**, 15160–15164.
154 C. J. Lu, M. M. Zhang, D. T. Tang, X. Z. Yan, Z. Y. Zhang, Z. X. Zhou, B. Song, H. Wang, X. P. Li, S. C. Yin, H. Sepehrpour and P. J. Stang, *J. Am. Chem. Soc.*, 2018, **140**, 7674–7680.

155 Z. K. Wang, J. Y. Nie, W. Qin, Q. L. Hu and B. Z. Tang, *Nat. Commun.*, 2016, **7**, 1–8.
156 Q. M. Liu, Q. Xia, S. Wang, B. S. Li and B. Z. Tang, *J. Mater. Chem. C*, 2018, **6**, 4807–4816.
157 H. Q. Peng, B. Liu, P. F. Wei, P. F. Zhang, H. K. Zhang, J. F. Zhang, K. Li, Y. Li, Y. H. Cheng, J. W. Y. Lam, W. Zhang, C. S. Lee and B. Z. Tang, *ACS Nano*, 2019, **13**, 839–846.
158 J. Li, K. Liu, H. Y. Chen, R. Y. Li, M. Drechsler, F. Bai, J. B. Huang, B. Z. Tang and Y. Yan, *ACS Appl. Mater. Interfaces*, 2017, **9**, 21706–21714.
159 J. J. Li, Y. Chen, J. Yu, N. Cheng and Y. Liu, *Adv. Mater.*, 2017, **29**, 1701905.
160 L. X. Xu, Z. Y. Wang, R. R. Wang, L. Y. Wang, X. W. He, H. F. Jiang, H. Tang, D. R. Cao and B. Z. Tang, *Angew. Chem., Int. Ed.*, 2019, **58**, 1–6.

Published on 23 January 2020. Downloaded by Yunnan University on 8/9/2025 11:18:24 PM.

This journal is © The Royal Society of Chemistry 2020